Betreuer

DIPLOMARBEIT

PHASE TRANSITIONS OF PATCHY COLLOIDS IN TWO DIMENSIONS

AUSGEFÜHRT AM
INSTITUT FÜR THEORETISCHE PHYSIK

BETREUER
GERHARD KAHL

DURCH

SUSANNE WAGNER
MATR.NR.: 1125888
SUSANNE.WAGNER@TUWIEN.AC.AT

21. Februar 2017

Studentin

TECHNICAL UNIVERSITY OF VIENNA

Abstract

Faculty of Physics
Institute of Theoretical Physics

Phase Transitions of Patchy Colloids in Two Dimensions

by Susanne WAGNER

In this thesis I study a two dimensional system of patchy colloids restricted to closest packing and its phase transition from an orientationally ordered into a disordered phase. I approached this problem by first defining orientational order by determining bonding patterns that emerge at low temperatures for different sizes of the patch. As the temperature is increased bonds start to break and this transition is studied via a suitable order parameter.
The systems were investigated via Monte-Carlo simulations. In order to identify the emerging bonding structures, a density and a cluster size analysis were employed. For the case where particles can form up to one bond (dimers), an order parameter was defined. With this order parameter at hand a correlation function was defined and was calculated for different temperatures in order to study the spatial range of the order in different phases.

Contents

Chapter 1

Introduction

Universality is a characteristic feature of phase transitions that demonstrates that to a considerable degree the critical behaviour often only depends on the dimensionality of the system, and not on the specific microscopic forces [17]. Therefore, phase transitions of systems in two dimensions often exhibit a fundamentally different behaviour compared to their three-dimensional counterparts. One transition that has been studied in detail is the two dimensional solid-liquid transition of colloid particles.

The fundamental theory, which is able to describe the melting of a two-dimensional solid of particles by topological defect unbinding was developed in the 1970s by Kosterlitz, Thouless, Halperin, Nelson and Young (KTHNY theory) [20][11]. This concept predicts the occurrence of an additional intermediate phase, the so-called hexatic phase, which emerges as an additional phase between the liquid and solid states. While the ordered tetragonal lattice in two dimensions has a six-fold rotational symmetry and a discrete translational symmetry, these discrete symmetries are lost during melting in favour of continuous symmetries in the liquid phase. For the intermediate phase the translational symmetry is already continuous while its six-fold rotational symmetry is still discrete. Because of the still remaining six-fold rotational symmetry in the intermediate phase, the latter one is called hexatic. This feature of the solid-liquid phase transition is completely unique for the two-dimensional case while in three dimensions the corresponding phase transition is a conventional first-order transition with no intermediate phase [7].

Some predictions of KTHNY theory, such as the existence of the hexatic phase were observed in simulations of the NVT-ensemble using different methods like the event-chain Monte-Carlo algorithm, a parallel form of local Monte-Carlo algorithm or event-driven Molecular Dynamic Simulation [4]. Also experimental groups were able to show the occurrence of the predicted hexatic phase using video-microscopy in a system of superparamagnetic colloid particles (with diameters of $4.5\mu m$) confined to a water-air interface [7].

Motivated by these fascinating theoretical and experimental findings of the phase transition of colloid particles in two dimensions, I wanted to study in my thesis the phase transition of a related two-dimensional system where the particles are characterized by an additional, rotational degree of freedom. For this purpose I assigned a patch with an attractive potential to the otherwise repulsive surface of the colloid particles. For simplicity the attractive potential is a step-well interaction, i.e. the simplest form of a short-range potential. Through patch overlaps the particles have the ability to form bonds.
The relevant question for this work was to find whether this orientational degree of freedom also gives rise to some temperature-dependent order in the orientation of the particles and to classify the transition from the rotationally ordered to the disordered phase when the system is heated up.

Both, experimentalists and theoreticians have already worked on this system or on related models.
For example, there have been experimental studies on the crystal formation of so-called AB Janus particles, which carry two opposite patches, in two dimensions. Here, due to entropic reasons, open crystal lattices such as the Kagome lattice have been formed [14]. But also systems of one-patch Janus particles have been subject to experiments. Here the authors of [8] were able to experimentally realize highly ordered zigzag stripe patterns in a monolayer.
Also theoretical work has been dedicated to the two dimensional patchy particle model which forms the basis of this work. Adapted from the Einstein solid, H. Shin and K.S. Schweizer [18] formulated a harmonic potential for particle vibrations and rotations in the two dimensional crystal of patchy particles. The spring constants were computed in a self-consistent manner. In this way, the authors were able to derive the free energy contributions for competing phases. With this information they were able to plot phase diagrams for crystals with high packing fractions.

Mostly by their work, I was inspired to study exactly these phase transitions in simulations and to gain a better understanding of how the system is undergoing the transitions between different phases.
In this work, I focused on the case where the particles are restricted to closest spatial packing. Thus, the phase transition governed by the loss of orientational order an be disentangled from the conventional liquid-solid transition. I first identified the possible ordered phases for patchy particles with different patch sizes. I used standard Monte-Carlo simulation to simulate systems with various patch and particle sizes at different temperatures. For analysing the emerging bond structures, a density and a cluster size analysis was employed. An order parameter was defined for particles

with patch sizes such that they can form up to one bond. With this order parameter at hand, a correlation function was defined in order to study the range of order in the different phases. Finally, also the heat capacity was calculated to obtain more information about the possible emergence of a phase transition.

Chapter 2

The Patchy Particle Model in Two Dimensions

2.1 The Kern-Frenkel Patchy Model

This model for a patchy colloid (figure 2.1) is a commonly employed model in soft matter theory. Its idea is to assign an additional patch with an attractive potential to the particles which breaks the rotational symmetry. The potential is attractive and short-range and therefore designed such that overlapping patches will form a bond. The type of the attractive potential in this work has been chosen to be a step-well potential. This is the simplest type for a short-range potential. Patchy particles with this type of potential are also known as Kern-Frenkel patchy particles [9]. The step-well potential V_{ij} is defined for two particles with indices i and j and distance vector $\vec{r}_{ij} = r\hat{r}_{ij}$ and with respective patch orientation vectors $\hat{\Omega}_i$ and $\hat{\Omega}_j$ with respect to an arbitrary but fixed axis as follows:

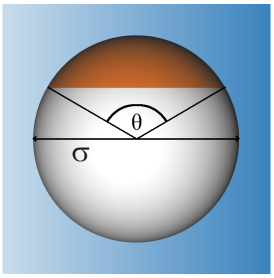

FIGURE 2.1: Model Particle

$$V_{ij}(\vec{r}_{ij}, \hat{\Omega}_i, \hat{\Omega}_j) = \begin{cases} +\infty & 0 < r < \sigma \\ -\epsilon V_\Phi(\hat{r}_{ij}, \hat{\Omega}_i, \hat{\Omega}_j) & \sigma < r < \sigma + \delta \\ 0 & \sigma + \delta < r \end{cases} \tag{2.1}$$

$$V_\Phi(\hat{r}_{ij}, \hat{\Omega}_i, \hat{\Omega}_j) = \begin{cases} 1 & \text{if } \hat{r}_{ij}\hat{\Omega}_i > \cos(\frac{\theta}{2}) \text{ and } \hat{r}_{ji}\hat{\Omega}_j > \cos(\frac{\theta}{2}) \\ 0 & \text{otherwise} \end{cases} . \tag{2.2}$$

The parameters of the model are the patch amplitude θ, the potential depth ϵ and the interaction range of the patches δ.
The value of the potential depth ϵ will determine the temperature scale. As I have restricted the problem to a spatial closest packing of spheres, the interaction range

becomes redundant in the present study. In the spatial closest packing of spheres in the two dimensions the particles form a tetragonal lattice.
The most important model parameter in this is the patch amplitude θ which determines up to how many bonds one particle can form. A particle that has one bond only can get a second one if the patch amplitude exceeds the angle of $(2\pi)/6$. The general condition for a particle with patch amplitude θ to form up to n bonds is:

$$\frac{\pi}{3}(n-1) < \theta < \frac{\pi}{3}n \tag{2.3}$$

2.2 Ground States of the system

In the studied model the particles are restricted to spatially closest packing. The model is purely two dimensional. Therefore, no rotations of the particles out of the xy plane are allowed. (This is emphasized here because the figures show a three dimensional rendering of the system.)
In an effort to define orientational order, the ground states, i.e. the states of lowest energy, have to be defined for different patch amplitudes. To obtain the state of lowest energy, the only constraint to the particles is that every particle must bond to the maximum number of possible bonding partners.
In the following, it will be helpful looking at the bonding patterns of the system instead of the real particles. In these patterns, lines between points represent the bonds formed by two particles. These patterns contain enough information about the system even though the exact information about each particle's orientation is lost.
When the particles can form one bond each ($n = 1$), they will bond into pairs. In the ground state these pairs will be distributed over the tetragonal lattice such that all particles are involved in exactly one bond (figure 2.2). For the reason that a number of configurations can be found, fulfilling this constraint, the ground state is highly degenerate. In the following I will not refer to pairs but to dimers. This is how the bond of two particles is called.
When $n = 2$, there are two possible patterns where to each particle two binding partners are assigned. Either, clusters of three particles will be formed or the particles will arrange along lines. These two patterns are shown in figure 2.2. Also any mixture of these two kinds is a valid ground state, as long as the lines are closed and every particle forms two bonds. Here, the bonds between three particles will be referred to as a trimer from now on.

The ground state in the case of $n = 3$ is are zigzag-lines figure 2.3. In contrast to the lines in figure 2.2, zigzag-lines can appear in two different types. I distinguish between left- and right tilted zigzag-lines. These lines can also change their direction

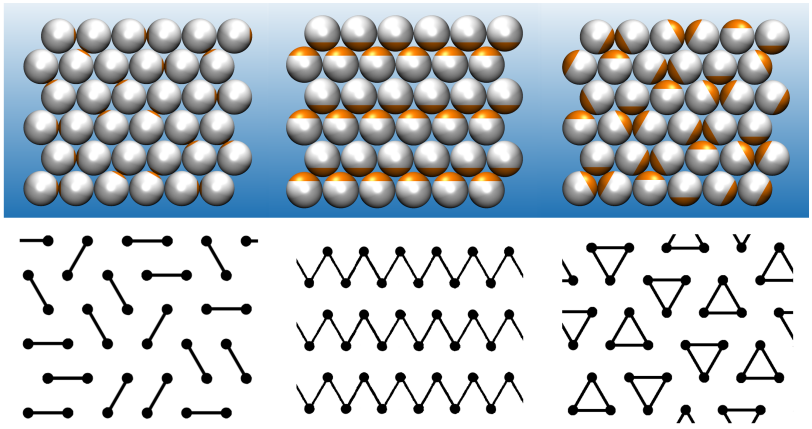

FIGURE 2.2: Ground states for $n = 1$ showing dimers (left) and for $n = 2$ showing lines and trimers (middle and right).

by $\frac{\pi}{3}$. But the possibility of a kink in one direction depends on the inner structure of the zigzag-lines, hence whether the line is a left- or right tilted zigzag-line. While left tilted zigzag-lines can take right turns, right tilted ones can take left turns. In this case the ground state is not as highly degenerate as in the dimer and in the trimer case. The lines are either all straight and the number of possible states is $2^{\#lines}$ or a kink appears but then all lines will have to be of one kind.

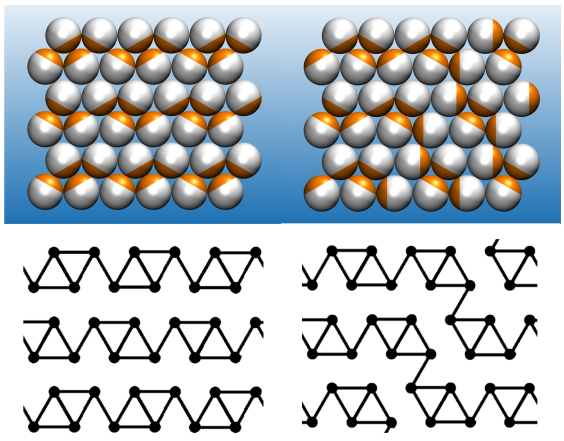

FIGURE 2.3: Ground states for $n = 3$ showing left and right tilted zigzag lines (left) and zigzag lines with a kink (right).

All other cases of ground states where $n > 3$ are already covered because they are just the inverted patterns to the ground states that have already been found for $n < 3$. Starting from the $(6 - n)$-ground state and inverting the pattern by replacing all bonding-axes by non-bonding-axes and vice versa, the ground states can be found for the cases where $n > 3$. Figure 2.3 shows the ground states for $n = 4$ and 5 derived from the ground states where $n = 2$ and 1, respectively.

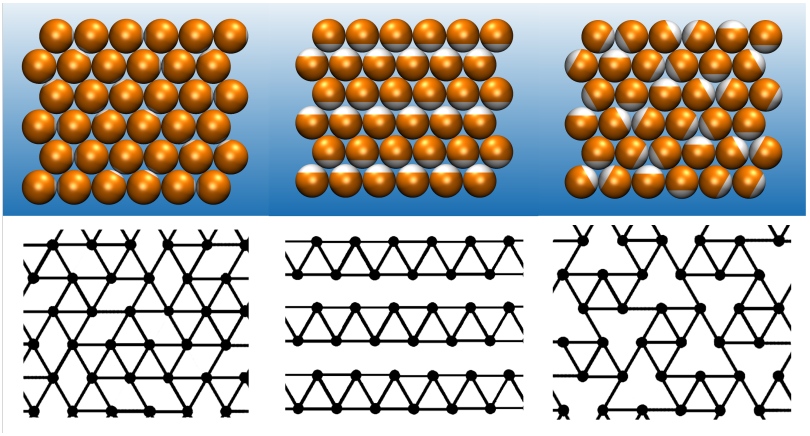

FIGURE 2.4: Ground states for $n = 4$ (left) and for $n = 5$ (middle and right) all showing the inverse patterns of figure 2.2.

2.3 Order-Disorder

All ground states discussed above are representing different ordered phases. The order-disorder transition in the system is driven by breaking bonds. A way of defining the order in a system is to define an order parameter. The order parameter that I was looking for has to fulfill the following requirements: First of all, by definition its magnitude should be a number between zero and one. Secondly, it should be maximal for the ideally ordered phase and considerably lower than one or zero for the disordered phase. For the dimer-case, the energy per particle ϵ was found to be a suitable order parameter. In the completely ordered phase, where every particle has one bond, $|\epsilon| = 1$. For higher temperatures where bonds start to break, the magnitude of the order parameter will drop and $|\epsilon| < 1$.

2.4 Thermodynamics of the System

I consider a system with a fixed particle number N, a fixed volume V and at a fixed temperature T. Therefore, the system is described in the canonical ensemble or synonymously in the NVT-ensemble. As it will be later shown (Chapter 2) the thermodynamic potential for this ensemble is the free energy F, and therefore the state of lowest free energy is the equilibrium state. The free Energy is a function of the particle number N, the volume V and the temperature T. It is obtained from a Legendre transform of U, i.e. the internal energy and the thermodynamic potential in its natural variables N, V and S, where S is the entropy.

$$F(N,V,T) = U(N,V,S) - TS(T) \tag{2.4}$$

At $T = 0$, the free energy reduces to the internal energy. Therefore, the equilibrium state or the state of lowest free energy is one of the ground states, which I specified in the previous section.
To understand why the system is undergoing a transition it must be understood that the internal energy U and the entropy S always have to be balanced in such a way that the total free energy is minimized. Therefore, a non-trivial competition between the entropy and the energy determines the phase in which the system appears. In general the entropy has to grow as the internal energy grows, otherwise the system would not undergo a transition. Therefore, as the temperature is increased, a kind of 'entropic force' makes the internal energy grow by letting bonds break. Due to the higher number of possible configurations as bonds have broke, the entropy increases and thus lowers the free energy. This bond breaking only proceeds as long as the increase of the entropic factor outweighs the increase in energy. But as the temperature rises the entropy gains weight against the internal energy and more bonds will break.

On the Entropy of the System

The entropy in the system has two contributions. First, the rotational entropy S_{rot} and secondly the configurational entropy S_{conf}.
The configurational entropy denotes the kind of entropy that arises from the number of possible configurations of bonding patterns across the lattice that are compatible with a fixed internal energy, and therefore with a fixed number of existing and broken bonds.
For the rotational entropy only the number of configurations of the individual particles compatible with a fixed bonding pattern is considered. A particle with n bonds has a rotational freedom, hence it can freely rotate by an angle ω_{free} (2.5) without loosing one of the existing bonds

$$\omega_{\mathrm{free}} = \theta - \frac{\pi}{6}(n-1)\,. \tag{2.5}$$

This rotational freedom gives rise to a number of configurations that are all compatible with the underlying bonding pattern. This number of configurations again are important for the rotational entropy. If a bond breaks the rotational freedom becomes mostly larger and the the number of configurations increases.

Chapter 3

On Classical Thermodynamics and Phase Transitions

3.1 Classical Thermodynamics

Classical thermodynamics has its origin in times when it was generally believed that heat is a kind of fluid that can flow from one body to another. In 1824, just on the basis of this heat-fluid theory Carnot was very well able of deriving limitations for the transformation of heat into work and vice versa. Essentially, this work is now known as the second law of thermodynamics. Only eight years later, Robert Mayer formulated the first law of thermodynamics which states the equivalence of heat to mechanical work. In the first half of the 19th century, physicists were looking for an explanation why heat was equivalent to energy on a microscopic level. They were connecting the heat of a body to the dynamical energy of molecules and atoms in it. This kinetic interpretation would suggest that all properties of a body could be known by considering the kinetics of the underlying atoms. But the sheer impossibility of treating a many-body-problem with such a great amount of particles within classical mechanics, lead to a statistical treatment of this ensemble of particles. The theory was mainly developed by Maxwell, Boltzmann and Gibbs and is known as Statistical Mechanics, which we will have a closer look on in chapter 3.1 [5, p.ix]. The extension of the theory by also considering quantum particles is covered by Quantum Statistics.
However, now I want to briefly summarize some theoretical concepts of classical thermodynamics. Mostly only those aspects which will be of importance in the further discussion of the topic.
Classical thermodynamics is designed to describe macroscopic thermal properties and how they are related to each other in a system through thermodynamic potentials and thermodynamic state variables. Macroscopic properties such as the temperature T, the pressure P or the volume V are important state variables in thermodynamics. An additional state variable is the entropy S, where the change of entropy of a system is defined as the change of heat when cooled or heated, divided by the

current temperature:

$$dS = \frac{\delta Q}{T} \,. \tag{3.1}$$

One distinguishes between extensive and intensive thermodynamic variables, where extensive variables are proportional to the particle number N while intensive variables are not. Temperature T and pressure P, which are intensive variables are first derivatives of the energy and therefore also referred to as external forces. Extensive variables are for example the volume V or the entropy S of the system. There is always a pair of conjugate variables of one intensive and one extensive variable. The contributing term to the change of energy is then always the intensive variable times the change of its conjugate external variable [2, p.111].
Next to thermodynamic state variables there are also thermodynamic potentials which are functions that contain all thermodynamic information. A thermodynamic potential contains the full information if it is written in its natural variables. The internal energy U is such a thermodynamic potential and has the extensive variables S, V and N as its natural variables. From derivatives of the potential with respect to the variables, the full set of thermodynamic properties of the system can be obtained [2, p.112].

Depending on the physical access (experiment, simulation or theory) it might be preferable to consider another potential, depending on another set of variables. Starting from the internal energy U one can obtain other valid thermodynamic potentials through Legendre transforms, one of which is the free energy F. This potential is defined in its natural variables as:

$$F(N, V, T) = U(N, V, S) - TS(T) \,. \tag{3.2}$$

While the internal energy U is the potential for a completely isolated system, a system that is in contrast not isolated but in contact with a heat reservoir allowing the systems to exchange heat Q, the appropriate potential is the free energy F. This can be easily seen from the second law of thermodynamics, which states that all changes (reversible and irreversible) in a system, when it is thermally isolated, are such that the change of entropy is positive. The entropy therefore always strives to be maximal. In the studied system which is in contact with a reservoir (primed variables) the total change in entropy is the sum of the change in the subsystems.

$$\Delta S_{\text{total}} = \Delta S + \Delta S' \geq 0 \,. \tag{3.3}$$

The heat reservoir is sufficiently large such that its temperature T' stays at a constant value $T' = T_0$ while heat is transferred. Therefore, $\Delta S' = \frac{\Delta Q'}{T_0} = -\frac{\Delta Q}{T_0}$, where ΔQ is the change of heat in the reservoir and $\Delta Q'$ the change of heat in the system. From the first law of thermodynamics we know that the total change of heat is the change of internal energy, ΔU plus the work $\Delta W = p_0 \Delta V$ that is done by the system. However, we do not allow volume changes in our system, therefore it is not able to perform work. All in all, relation (3.3) then becomes:

$$\Delta S - \frac{\Delta U}{T_0} \geq 0 \tag{3.4}$$

$$\Delta \left(U - T_0 S \right) \leq 0 \tag{3.5}$$

$$\Delta F \leq 0 \tag{3.6}$$

Therefore, the free energy of a system that is in thermal contact with a reservoir is striving to be minimal. Hence, the system is in equilibrium only if F is minimized. The same derivation leads to the minimization of the Gibbs free energy, G if temperature and pressure are fixed. This is a system where exchange of heat and volume with a reservoir is allowed. A completely isolated system (internal energy U, Volume V and particle number N fixed) tries to maximize its entropy [2, p.113].

3.2 Phase Transitions

Definition of a Phase

Matter can appear in different phases or aggregate states. The surrounding conditions like pressure, temperature, magnetic and electric fields determine in which phase the material will exist. In a system with a given set of thermodynamic variables always the phase which minimizes the underlying thermodynamic potential will appear, like it was derived for the free energy, F in the previous section [17, p.333]. It is also possible that two or more phases coexist under the given thermodynamic variables [16, p.98].
Symmetries play an important role in the theory of phase transitions. Phases have different symmetry properties and therefore differ in their thermal and mechanical behaviour. In a liquid phase the system has continuous translational symmetry and also continuous rotational symmetry. This is because the liquid is invariant under

such transformations. Or equivalently, one can say, the liquid looks the same at every position and in every direction. These symmetries however are not preserved as the liquid crystallizes into a solid. In the solid state the crystal possesses only discrete symmetries such as discrete translational symmetry and discrete rotational symmetry, depending on the lattice type of the crystal. Both phases have different symmetries and as mentioned before, these symmetries define the mechanical and thermal properties of the phases.
It is often referred to a high-temperature disordered and a low-temperature ordered phase. It is generally true for phase transitions that during the transition from a high-temperature phase with high symmetry into a low-temperature phase with low symmetry, the symmetries are broken in one ore more steps [7, p.41].

Critical Point and Order Parameter

As the critical point one defines the point where a new phase begins to appear. The appearance of the new phase is connected to the appearance of its order parameter [16, p.135]. And the order parameter itself is closely connected to the symmetry of the respective phase. As the order parameter is a measure for the symmetry related order in the specific phase. Approaching the critical point from above (from the higher temperature) the order parameter of the new phase is first zero and only starts to grow continuously when the critical point is reached [17, p.339].

Ehrenfest classification

The phase transition itself is most commonly classified based on the behaviour of the derivatives of the thermodynamic potential at the transition point as it was proposed by Ehrenfest. A phase transitions is according to Ehrenfest a phase transition of n-th order, if at least one n-th derivative of the thermodynamic potential with respect to a thermodynamic variable is discontinuous and all lower derivatives are continuous [17, p.334].

First-order phase transitions are therefore phase transitions in which the first derivative of the thermodynamic potential is discontinuous. Examples for this type of phase transitions are provided by the vapor-liquid, the liquid-solid and the vapor-solid transition in classical fluids [16, p.96].
Phase transitions in which the change of state is continuous will have a discontinuity in the second or in a higher derivative of the potential. Second-order phase transitions in which a second derivative of the potential is discontinuous are therefore also referred to as continuous phase transitions [16, p.96].

In the canonical ensemble, where the temperature and the volume is kept constant, the free energy, F is the respective thermodynamic potential. First derivatives of the free energy are given by the pressure and the entropy. In the case of a first order transition, a discontinuity occurs in at least one of these quantities.
For the canonical ensemble the specific heat at constant volume C_V is a second derivative of the thermodynamic potential F. If the transition is continuous there might be a discontinuity in C_V at the point of transition. However, for a transition of first order, the second derivative is a derivative of a discontinuous quantity and therefore the transition will be characterized by a very high and sharp peak (or an infinite peak) in the specific heat C_V.

The Ehrenfest classification is however not universal since there are systems for which some higher-order derivatives are infinite. For these systems the classification breaks down [16, p.101].

Correlation Functions and Order Range

The process of loosing order when a phase transition from an ordered to a disordered phase is taking place can also be monitored by the use of correlation functions. Typically one looks at the correlation function of the order parameter. The correlation length and the type of decay of the correlation function is characteristic for a phase. In ordered phases the system typically exhibits long-range or quasi long-range order. In a solid-liquid transition the positional order is measured by the pair-correlation function of the particles $g(r) = \langle \rho(r)\rho(0) \rangle$. In the liquid phase it exhibits short-range order due to the fact that the correlation function decays exponentially. On the other hand a perfect crystal reveals quasi long-range behaviour meaning that the decay is according to a power-law. For real long-range order the correlation function would be constant.

Behaviour at the Critical Temperature

At the critical point and in its vicinity, the system begins to exhibit a new behaviour. As the critical point is approached fluctuations in density, magnetization or in general in fluctuations of the order parameter appear. These fluctuation essentially diverge in their extent at the critical point itself. Below the critical point the new phase has formed and the corresponding order parameter becomes nonzero.

Universality

From experiments and computer simulations on various systems, it was found that very different systems may exhibit the same critical behaviour. This same critical behaviour can be seen directly from the topological similarities in the phase diagrams but especially from the critical exponents. In the vicinity of the critical point the temperature dependent behaviour of a thermodynamical function is described by a power law with a critical exponent. Systems that have the same set of critical exponents for different thermodynamical functions are forming a universality class [16, p.136].
The general definition of a critical exponent with a thermodynamical function $f(\tau)$ is given by:

$$\alpha = \lim_{\tau \to 0} \frac{\ln(f(\tau))}{\ln(\tau)} \tag{3.7}$$

Here $\tau = \frac{T - T_c}{T_c}$ is a dimensionless temperature that vanishes at the critical point T_c.
The reason for universality was found to be the divergence of the correlation length at the critical point. As the correlation length diverges it becomes the only relevant length scale in the system. Therefore, microscopic features like the type of the potential, as long as it is short-ranged, and the lattice properties do not play any role at the critical point anymore. The properties of the system that determine the type of transition are the global ones, like the dimensionality of the system, the dimension of the order parameter, the number of degrees of freedom and the symmetry [17, p.341][7, p.42].
The phenomenon of universality and scale invariance at the critical point is the central topic of renormalization group theory, which I will not discuss here. Within this theory the scale of the system is subsequently renormalized until a fixed point or an interaction free system is obtained [17, p.348].

3.3 Melting Transition in 2 dimensions for Colloid Particles

In contrast to three-dimensional systems, there exist microscopic theories for the solid-liquid transition in two dimensions for systems of colloid particles.
While there are theories suggesting grain-boundary induced melting [3][10] or condensation of geometrical defects [6], KTHNY theory (named after Kosterlitz, Thouless, Haldane, Nelson and Young) is based on the idea that the transition is driven by unbinding of topological defects (Grünberg, Keim, Maret, p.43). A single defect on a two-dimensional lattice is called a topological defect if there is no continuous

transformation that would make this defect disappear. Therefore, topological defects can only appear pairwise [7, p.44]. The KTHNY-theory predicts a transition from the solid to the liquid phase through an intermediate phase, which is called hexatic phase. The transition from the solid to the hexatic phase is driven by the unbinding of one type of topological defects which are dislocations. Through the dissociation of the dislocation the translational symmetry of the solid phase is destroyed. There is also another type of topological defects which are disclinations. These defects destroy rotational symmetry in a second transition step where the hexatic phase is changing into the completely isotropic liquid phase. The intermediate phase originates from the different activation energies for the unbinding of the dislocations and the disclinations.

As already indicated, the hexatic phase is characterized by continuous translational symmetry and a remaining local six-fold rotational symmetry. By contrast, the solid phase has both discrete translational and rotational symmetry and the liquid phase has only continuous symmetries. While the order parameters are a measure for the local symmetries in the system, the range of order of the symmetry properties in a phase can be observed in the correlation functions of the order parameters. The local orientation order parameter, $\psi_k = \langle e^{6i\phi_{kl}} \rangle$, for a particle with index k measures the local six-fold rotational symmetry when averaged over all neighbours l of k. The orientational correlation function $g_6(r) = \langle \psi(r)\psi(0) \rangle$ then characterizes the range of orientational order in the system. In contrast, the range of positional order is measured by using the positional pair correlation function, $g(\Delta r) = \langle \rho(r)\rho(r+\Delta r) \rangle$ with the particle density $\rho(r)$.

KTHNY-theory predicts short-range positional order and long-range orientational order for the hexatic phase. The tetragonal lattice of the solid phase exhibits quasi long-range positional order and long-range orientational order. All these predictions were confirmed in experiments and in simulations [7][4].

Chapter 4

On Statistical Mechanics and Monte-Carlo Simulations

4.1 Statistical Mechanics

4.1.1 Introduction

In contrast to classical thermodynamics (Chapter 2.1) which deals with the macroscopic properties of a system, statistical mechanics is a probabilistic microscopic theory. The most essential and important relation between the micro- and the macroscale was made by Boltzmann who discovered the relation between the number of possible microstates Ω compatible with the given macroscopic parameters, and the entropy S:

$$S \propto \ln(\Omega) \tag{4.1}$$

The general aim of statistical mechanics is the derivation of macroscopic properties that are accessible in an experiment from the statistical treatment of the microscopic system and its underlying Hamiltonian [16, p.285]. Measurable properties or physical interesting properties are the specific heat-capacity, the thermal expansion coefficient, heat conductivity or electric conductivity, to name a few examples.

Phase Space in Statistical Mechanics

When considering a classical system with N spherical particles in three dimensions the independent coordinates or degrees of freedom are $3N$ space coordinates and $3N$ coordinates for the momenta of the particles. Every state of the system is defined by $6N$ coordinates and the space spanned by these coordinates is called phase space Γ [17, p.9]. In other words, phase space is a multidimensional space in which each point represents a microstate of the system [12, p.10]. The motion of a point in phase space is governed by Hamiltonian dynamics (Hamilton equations of motion). Anyhow, if the considered system contains a large number of particles N, we will

practically never be able to know the exact state of the system. All we may be able to know by using the tool of statistical mechanics is the probability of the system being in one certain state or more precisely the probability density, which will be denoted as ρ in the following, for the system occupying a certain phase space volume. This point of the sheer impossibility of knowing all the states of the N particles, is where classical mechanics is replaced by statistical mechanics, a probabilistic description of the microstates.

Ensembles

A microstate is a point in phase space which is defined for a classical system with N spherical particles by the $6N$ phase space coordinates $(q_{1i}, q_{2i}, q_{3i}, p_{1i}, p_{2i}, p_{3i})$, where i is the particle index that goes up to N. A macrostate on the other hand is defined by a set of macroscopic parameters like the energy, the volume or the temperature. All microstates compatible with one macrostate weighted with the respective probability with which they can occur in the Γ-space are called a statistical ensemble.

According to the macroscopic parameters that are kept constant, different statistical ensembles are defined [17, p.3]. In Chapter 2 where systems were put in contact with heat and/or particle reservoirs, in statistical mechanics the same procedure leads to different ensembles.
A completely isolated system which according to the second law of thermodynamics tries to maximize its entropy under the given boundary conditions is described within the microcanonical ensemble in statistical mechanics. The equilibrium state for this system is the state with highest entropy. It is a time-independent state and it can be described by only a few thermodynamic state variables. Another name for it is UVN-ensemble, which names the ensemble after the thermodynamic variables that are kept constant.
Since it is rather hard to experimentally keep the internal energy U constant, a system is preferred where instead the temperature is kept constant. This is achieved by putting the system into contact with a thermal reservoir of a fixed temperature and allowing the exchange of heat between the system and the reservoir. Note that since the volume is constant heat and energy are equal. The corresponding ensemble in statistical mechanics is the canonical ensemble, or NVT-ensemble.
Other ensembles are the grand canonical ensemble, or μVT-ensemble where also exchange of particles with the reservoir is allowed, the isothermal-isobaric ensemble or NPT-ensemble where additionally the system can undergo volume changes.

The simulations on the model-system studied in this thesis were all performed in

the canonical ensemble which is why I will continue considering the microcanonical and the canonical ensembles.

4.1.2 The Ergodic Theorem

A state vector $\mathbf{X}^N$ in phase-space is defined by the three position and three momentum coordinates of all N particles of a system $\left(\mathbf{q}^N, \mathbf{p}^N\right)$. The Hamiltonian $\mathcal{H}(\mathbf{q}^N, \mathbf{p}^N)$ defines the evolution of this state vector in phase space by the Hamiltonian equations of motion (4.2).

$$\frac{d\mathbf{q}_i}{dt} = \frac{\partial \mathcal{H}(\mathbf{q}^N, \mathbf{p}^N)}{\partial \mathbf{p}_i} \qquad \frac{d\mathbf{p}_i}{dt} = -\frac{\partial \mathcal{H}(\mathbf{q}^N, \mathbf{p}^N)}{\partial \mathbf{q}_i} \tag{4.2}$$

The evolution of such a state vector $\mathbf{X}^N$ with fixed energy, U will then be restricted to a $6N-1$ dimensional hyper-surface of constant energy in phase space. The flow on the energy surface is called ergodic if almost all trajectories $\mathbf{X}^N(t)$ sample small neighbourhoods on the entire energy surface.

The **ergodic theorem** states that a system is ergodic if the time average $\langle f \rangle_T$ for all functions $f(\mathbf{X}^N)$ on phase space exists for almost all $\mathbf{X}^N$ and is equal to the phase space average $\langle f \rangle_S$. The time and phase space average for a function $f(\mathbf{X}^N)$ are defined by:

$$\langle f \rangle_T = \lim_{T\to\infty} \frac{1}{T} \int_{t_0}^{t_0+T} f(\mathbf{X}^N(t))dt \tag{4.3}$$

$$\langle f \rangle_S = \frac{1}{\Omega(U)} \int_\Gamma \delta(U - H^N(\mathbf{X}^N)) f(\mathbf{X}^N) d\mathbf{X}^N \tag{4.4}$$

The phase space average is the integral of the function on the surface of constant energy in phase-space Γ. Here $\Omega(U)$ is the area of the respective energy surface [16, p.296].

4.1.3 The Probability Density Function

In this section I derive the probability densities for the microcanonical and the canonical ensemble. The probability density function $\rho(\mathbf{X}^N)$ should be normalized over the whole phase space Γ:

$$\int_\Gamma d\mathbf{X}^N \rho(\mathbf{X}^N) = 1 \tag{4.5}$$

And it should give the probability for a system being in a state that is in a subregion R of phase space Γ by integration over this subregion:

$$p(\mathbf{X}^N \in R) = \int_R d\mathbf{X}^N \rho(\mathbf{X}^N)\,. \tag{4.6}$$

Micro Canonical Ensemble

For ergodic flow, almost all points $\mathbf{X}^N$ sample all finite neighbour regions R_E on the energy surface. As a consequence the system spends equal times in regions of equal extent. The corresponding probability for a microstate $\mathbf{X}^N$ to appear is therefore naturally a uniform distribution. It is postulated that every microstate $\mathbf{X}^N$ with energy U is equally probable and therefore the probability density is given by:

$$\rho(\mathbf{X}^N, U) = \frac{\delta(U - \mathcal{H}(\mathbf{X}^N))}{\Omega(U)}\,. \tag{4.7}$$

Here, $\Omega(U)$ as specified in equation 4.8 is the area of the surface of constant energy U in phase space. $\Omega(U)$ is proportional to the total number of states compatible with energy U in a discrete system or quantized system

$$\Omega(U) = \int_\Gamma d\mathbf{X}^N \delta(U - \mathcal{H}(\mathbf{X}^N))\,. \tag{4.8}$$

Canonical Ensemble

Now we are interested in the probability density for the microstates in the canonical ensemble. In the canonical ensemble instead of a fixed internal energy U, the temperature T is kept constant. This is achieved by putting the system S_1 in thermal contact with a reservoir S_2 with constant temperature T_0. The combined system $S = S_1 + S_2$ is completely isolated and described by the microcanonical ensemble. The probability density for the combined system is given according to (4.7) by:

$$\rho(\mathbf{X}^N = (\mathbf{X}_1^N, \mathbf{X}_2^N), U = U_1 + U_2) = \frac{\delta(U - \mathcal{H}_1(\mathbf{X}_1^N) - \mathcal{H}_2(\mathbf{X}_2^N))}{\Omega(U)}\,. \tag{4.9}$$

To get the probability density for subsystem S_1, Equation (4.9) is integrated over all variables of subsystem S_2. Later the probability density has to be normalized such that $\int d\Gamma \rho = 1$.

$$\rho(\mathbf{X}_1^N, U_1) \sim \int_{\Gamma_2} d\mathbf{X}_2^N \frac{\delta(U - \mathcal{H}_1(\mathbf{X}_1^N) - \mathcal{H}_2(\mathbf{X}_2^N))}{\Omega(U)} \tag{4.10}$$

Here, the numerator gives according to (4.8) the surface area of all states with energy

$(U - \mathcal{H}_1)$ in sub-phase-space Γ_2.
The resulting expression,

$$\rho(\mathbf{X}_1^N, U_1) \sim \frac{\Omega_2(U - \mathcal{H}_1(\mathbf{X}_1^N))}{\Omega(U)} \tag{4.11}$$

can be further simplified by expanding under the assumption that $U_1 << U$. This is justified by the fact that the heat reservoir S_2 is assumed to be much bigger than S_1. Ω_2 can be rewritten as $\exp(\ln \Omega_2)$. In the next step the emerging logarithm is expanded for $U_2 \approx U$:

$$\begin{aligned}
\Omega_2(U_2) &= e^{\ln \Omega_2(U - H_1)} \\
&= \exp\Big[\, ln\Omega_2(U_2)|_{U_2=U} + \frac{\partial \ln \Omega_2(U_2)}{\partial U_2}\Big|_{U_2=U} (U_2 - U) + ...\Big] \\
&= \exp\Big[\ln \Omega_2(U) - \frac{\partial \ln \Omega_2(U_2)}{\partial U_2}\Big|_{U_2=U} H_1 + ...\Big]
\end{aligned} \tag{4.12}$$

Given the identities for the entropy introduced in (3.1) and in (4.1) with the correct proportionality,

$$S = k_B \ln(\Omega) \qquad\qquad dS = \frac{\delta Q}{T} \tag{4.13}$$

(4.12) can be further simplified:

$$\begin{aligned}
\Omega_2(U_2) &= \Omega_2(U) e^{-\frac{1}{k_B}\frac{\partial S_2}{\partial U_2}\mathcal{H}_1} \\
&= \Omega_2(U) e^{-\frac{\mathcal{H}_1}{k_B T}} .
\end{aligned} \tag{4.14}$$

Bear in mind that $dQ = dU$ in the microcanonical ensemble where the volume V is kept constant.
The desired probability density for the subsystem S_1 is then given by:

$$\rho(\mathbf{X}_1^N) \sim \frac{\Omega_2(U)}{\Omega(U)} e^{-\frac{\mathcal{H}_1(\mathbf{X}_1^N)}{k_B T}} . \tag{4.15}$$

The factor $e^{-\frac{\mathcal{H}_1}{k_B T}}$ is called Boltzmann-factor. The other factor in (4.15) is a constant and independent of the subsystem S_1. Therefore it drops out when the distribution is normalized.

After normalization and having dropped the indices for subsystem S_1, the probability density for a system with Hamiltonian $\mathcal{H}$ in the canonical ensemble is given by [17, p.51]:

$$\rho(\mathbf{X}^N) = \frac{e^{-\frac{\mathcal{H}(\mathbf{X}^N)}{k_B T}}}{\int d\Gamma e^{-\frac{\mathcal{H}}{k_B T}}} \,. \tag{4.16}$$

4.1.4 The Partition Function and Expectation Values

While the probability density function $\rho(\mathbf{X}^N)$ for the microcanonical ensemble gives simply a uniform distribution for all microstates of the same energy U, in the canonical ensemble using $\beta = \frac{1}{k_B T}$ the probability density takes the form:

$$\rho(\mathbf{X}^N) = \frac{1}{Z} e^{-\beta \mathcal{H}(\mathbf{X}^N)} \,. \tag{4.17}$$

Here Z, the so-called partition function is the normalization factor given by:

$$Z = \int d\Gamma e^{-\beta \mathcal{H}} \,. \tag{4.18}$$

In the microcanonical ensemble the partition function gives the phase space volume $\Omega(U)$ as given in Equation (4.8).
The ensemble average for an observable $A(\mathbf{X}^N)$ in the canonical ensemble can then be written as:

$$\langle A \rangle = \frac{1}{Z} \int_\Gamma d\mathbf{X}^N A(\mathbf{X}^N) e^{-\beta \mathcal{H}(\mathbf{X}^N)} \,. \tag{4.19}$$

Sometimes the integral over phase space $d\Gamma$ is introduced including an additional factor $(h^{ND})^{-1}$. Here D is the dimensionality of the system and h an arbitrarily chosen constant. This factor is a normalization that clarifies/illustrates that each point in phase space $\mathbf{X}^N$ occupies a finite volume h^{ND}. However, the ensemble averages do not depend on this factor. Only the thermodynamic potentials such as the entropy will depend on it when it is introduced.
More importantly is another factor $(N)^{-1}$ that must be considered in the probability density, if the particles of the system are indistinguishable. It makes sure that a set of N microstates that can be transformed into one another by permutation of the particle indices are counted as only one microstate [17, p.27].

4.1.5 Heat Capacity from Fluctuations in Energy

In this section an expression for the specific heat will be derived from the expectation values for the Hamiltonian in the canonical ensemble.
The specific heat is defined as the change of internal energy δU with respect to the change of temperature δT. The internal energy is given by the expectation value of the Hamiltonian in the respective ensemble. In the canonical ensemble the expectation value for the Hamiltonian is calculated by weighting each energy by the Boltzmann factor $e^{-\beta\mathcal{H}}$. According to Equation (4.24) the internal energy is thus given by:

$$\bar{U} = \langle \mathcal{H} \rangle = \frac{1}{Z} \int_{\Gamma} d\mathbf{X}^N \mathcal{H}(\mathbf{X}^N) e^{-\beta\mathcal{H}(\mathbf{X}^N)} \,. \tag{4.20}$$

Similarily, the expectation value for $\mathcal{H}^2(\mathbf{X}^N)$ is defined as:

$$\bar{U^2} = \langle \mathcal{H}^2 \rangle = \frac{1}{Z} \int_{\Gamma} d\mathbf{X}^N \mathcal{H}^2(\mathbf{X}^N) e^{-\beta\mathcal{H}(\mathbf{X}^N)} \,. \tag{4.21}$$

Taking the derivative of Equation (4.20) with respect to β and identifying the upcoming terms with (4.20) and (4.21) leads to:

$$\frac{\partial \langle \mathcal{H} \rangle}{\partial \beta} = \langle \mathcal{H} \rangle^2 - \langle \mathcal{H}^2 \rangle \tag{4.22}$$

Writing $\beta = \frac{1}{k_B T}$ leads to a formula for the specific heat:

$$C_V = \frac{\partial \langle \mathcal{H} \rangle}{\partial T} = \frac{\langle \mathcal{H} \rangle^2 - \langle \mathcal{H}^2 \rangle}{k_B T^2} \,. \tag{4.23}$$

4.2 Monte-Carlo Simulations

Within Statistical Physics the most common application of Monte-Carlo method is to find reliable evaluations of the expectation values as given in equation (4.24). Only for a hand-full of physical systems the partition function is accessible via analytical expressions. For the overwhelming majority of systems numerical methods for the calculation of the integrals of the partition function and the expectation values have to be applied. Anyhow, the integral over phase-space represents an extremely high dimensional problem and therefore standard methods for numerical integration fail at this problem. This is where the Monte-Carlo method serves a practical tool. The

theory presented in the succeeding sections is based on [12].

4.2.1 Simple Sampling Monte-Carlo methods

In this section the core idea of Monte-Carlo sampling methods will be introduced. Considering a system with Hamiltonian $\mathcal{H}(\mathbf{X}^N)$ with continuous degrees of freedom in the canonical ensemble, the expectation value of some observable A is given by equation (4.24). Here the integral extends over all possible states $\mathbf{X}^N$ in phase space Γ and Z is the respective partition function.

$$\langle A \rangle = \frac{1}{Z} \int_\Gamma d\mathbf{X}^N A(\mathbf{X}^N) e^{-\beta \mathcal{H}(\mathbf{X}^N)} \,. \tag{4.24}$$

For a system with a discrete phase-space this expectation value can also be represented by a sum. For the patchy colloid particles restricted to closest packing the according expectation value of some observable $A(\vec{\theta_i})$ is given by:

$$\langle A \rangle = \frac{1}{Z} \int d\vec{\theta_i} A(\vec{\theta_i}) \cdot e^{-\beta \mathcal{H}(\vec{\theta_i})} \tag{4.25}$$

Note that the Boltzmann-factors $e^{-\beta \mathcal{H}(\mathbf{X}^N)}$ are just relative probabilities. The absolute probability for a state $\mathbf{X}^N$ is given by $p(\mathbf{X}^N) = \frac{e^{-\beta \mathcal{H}(\mathbf{X}^N)}}{Z}$. However, the partition function Z is not known. This will become important later in this chapter.

An approximate evaluation of Equations (4.24) or (4.25) can be achieved using Monte-Carlo method. Here, the core idea is to generate a number of configurations $\mathbf{X}_k^N$, with $k = 1, ..., n$ as a sample from phase-space. Using this sample, an approximation of $\langle A \rangle$ can be simply made by evaluating $A(\mathbf{X}_k^N)$ for each configuration and performing the summation over these values with their respective Boltzmann factors (see Equation (4.26)).

$$\langle A \rangle \approx \langle A \rangle_{MC} = \frac{1}{\sum_{k=1}^n e^{-\beta \mathcal{H}(\mathbf{X}_k^N)}} \sum_{k=1}^n A(\mathbf{X}_k^N) \cdot e^{-\beta \mathcal{H}(\mathbf{X}_k^N)} \,. \tag{4.26}$$

In this procedure the configurations are generated completely randomly. The sample originates therefore from a uniform distribution of all possible configurations. However, following this method a considerably large number of configurations will give a vanishingly low contribution to the sum in Equation (4.26) due to the fact, that the Boltzmann-factors can get very small. The integral or sum will therefore converge very slowly. This happens not only for the Boltzmann distribution but is

generally true for any integral of a highly varying function when applying Monte-Carlo integration method. The slow convergence then demands a larger sample and therefore longer computation times are required.

The sample standard deviation of this sample mean is given by:

$$\sigma(A) = \frac{1}{\sqrt{n-1}} \Big(\sum_{k=1}^{n} (A(\mathbf{X}_k^N) - \langle A \rangle_{\mathrm{MC}})^2 \Big)^{\frac{1}{2}} \tag{4.27}$$

Thus the standard error ϵ is given by:

$$\epsilon = \frac{\sigma}{\sqrt{n}} \tag{4.28}$$

The error can be derived by using the central limit theorem. This theorem states a general behaviour for the average value $\bar{x}_n = \frac{\sum_{i=1}^{n} x_i}{n}$ of independent random variables $x_1, x_2, ..., x_n$ which are drawn from the same distribution with the expected value μ and variance σ^2. The distribution is not further specified and need not be a Gaussian distribution.
In the limit of very large sample sizes n the central limit theorem states that the distribution of the sample averages $\bar{x}_n$ approaches the Gaussian distribution with expected value μ and variance σ^2/n. This leads to the error (4.28), which is given by the standard deviation of the sample means from the expected value μ. On the other hand, the standard deviation σ as given in (4.27) is a measure of the distribution of the random variables $A(\mathbf{X}_k^N)$ among the sample mean $\langle A \rangle$.
The dependence of the statistical error on the sample size n shows that when decreasing the statistical error by a factor of 10, one has to increase the sample size by a factor of 100.

One can also consider the error (4.28) and pose the question how it can be reduced. The two possibilities of doing that is to increase the sample size or to make the sample standard deviation as small as possible. How the latter can be achieved will be discussed in the next section.

4.2.2 Importance Sampling

A more efficient Monte-Carlo sampling method is importance sampling. Due to the fact that when sampling from a uniform distribution a large number of irrelevant contributions is generated, it would therefore be appropriate to preferentially generate configurations with large Boltzmann-factors, hence configurations with relevant

contributions to the expectation value.
When discussing the statistical error in Equation (4.28) it was stated that this quantity can be decreased by making σ small. This is achieved by sampling a set of $\mathbf{X}_k^N$ such that the deviations of $A(\mathbf{X}_k^N)$ from the mean become as small as possible. Therefore the aim of importance sampling is to find a probability distribution function such that this is achieved.

I want take a step backwards and outline the idea of importance sampling by regarding some general integral of some function $f(x)$ over the integration domain V as given in Equation (4.29)

$$I = \int_V dx f(x)\,. \tag{4.29}$$

The previously described sampling method, where random variables x are drawn from a uniform distribution, leads to a sum given in (4.30) as an estimate for I. It will converge slowly if $f(x)$ is a strongly varying function over the integration domain V. The error is given by $\sigma_f/\sqrt{n}$

$$I \approx \frac{1}{n}\sum_{k=1}^{n} f(x_k)\,. \tag{4.30}$$

The integrand is now expressed via two factors, i.e. $f(x) = g(x)p(x)$, with the aim that $g(x)$ becomes a slowly varying function. Fulfilling the condition $\int_V p(x) = 1$ and $0 < p(x) < 1$, $p(x)$ is a valid probability measure. Sampling x_k from $p(x)$ will then give the following approximtion to the integral with the error $\sigma_g/\sqrt{n}$.

$$I = \int_V dx g(x)p(x) \approx \frac{1}{n}\sum_{k=1}^{n} g(x_k) \tag{4.31}$$

The probability density $p(x)$ has to be chosen such that the statistical error σ_g for the approximation to the integral becomes as low as possible. The aim of this procedure was to reduce the sample standard deviation (Equation (4.27)) in order to achieve a smaller error. Choosing $p(x)$ such that it captures the features of $f(x)$ as good as possible, $g(x)$ becomes a function with low variations. Then it is generally true for the sample standard deviations that $\sigma_g < \sigma_f$.

Coming back to the initial problem of estimating the expectation value for some observable A, the same procedure can be followed. The integrand in Equation (4.24) is already factorized and $p(x) = e^{-\beta\mathcal{H}(x}/Z$ is a valid probability measure.
The estimate of Equation (4.24) when employing importance sampling is then given

by:

$$\langle A \rangle \approx \frac{1}{n} \sum_{k=1}^{n} A(\mu_k) \,. \tag{4.32}$$

The remaining task is to find a way to sample x_k from the given distribution $p(x) = e^{-\beta \mathcal{H}(x)}/Z$.

4.2.3 Markov-Chains and the Metropolis Algorithm

Now the task is to find a way of how to generate configurations from the given distribution $p(x)$. Because the absolute probability function is not known the task is to generate random variables with relative probabilities proportional to the Boltzmann-factor.

Markov-Chains

This can be done by using Markov-Chains. In a Markov-Chain without memory an ordered sequence of random variables $(x_{t_1}, x_{t_2}, ..., x_{t_n})$ is generated where each variable x_{t_k} depends on its predecessor $x_{t_{k-1}}$ only. The random variable x can take a value from a set of possible states denoted by $S_1, S_2, ...$. A Markov-chain can be generated introducing a transition probability $W_{i \to j} = W(x_{t_n} = S_j | x_{t_{n-1}} = S_i)$. This is a conditional probability for generating the new state S_j at the time t_n if the preceding one was the state S_i. The total probability $p_n(S_i)$ for finding state S_i at a time t_n is given by the Master equation:

$$p_n(S_j) = p_{n-1}(S_j) + \sum_i W_{i \to j} p_{n-1}(S_i) - \sum_i W_{j \to i} p_{n-1}(S_j) \,. \tag{4.33}$$

This relation is the formulation for discrete time steps. The equation can also be formulated for a continuous time scale where the resemblance to a continuity equation becomes more obvious.

In order to be able to use this relation for sampling from a given probability distribution $p(x)$, the task is to find a suitable transition amplitude $W_{i \to j}$. This transition amplitude must be designed such that first of all, the probability p_n reaches an equilibrium p_{eq} for large n and secondly, the resulting equilibrium probability is proportional to the desired probability distribution $g(x)$ specified in section 4.2.2.

Detailed Balance Condition

At equilibrium the time dependent probabilities p_n must not change from one time step to another. Therefore, $p_n(S_j)$ must be equal $p_{n-1}(S_j)$. Inserting this requirement into the Master equation (4.33) gives the global balance condition,

$$\sum_i W_{ji} p_{\mathrm{eq}}(S_j) = \sum_i W_{ij} p_{\mathrm{eq}}(S_i)\,. \tag{4.34}$$

The strongest balance condition that automatically satisfies the global balance condition is the detailed balance condition for which:

$$W_{ji} p_{\mathrm{eq}}(S_j) = W_{ij} p_{\mathrm{eq}}(S_i)\,. \tag{4.35}$$

Detailed balance is of high importance for standard Monte-Carlo simulations. It states that a transition from a configuration S_i to S_j has to be as likely as the backwards transition [12]. Anyhow, there are also weaker balance conditions between global and detailed balance that are sufficient for the Monte-Carlo sampling [13].

Metropolis Algorithm

The Metropolis Algorithm [15] uses the characteristics of Markov-Chains in order to generate a sample of configurations from a probability distribution proportional to the Boltzmann distribution. The configurations are therefore generated as a Markov-Chain, with the transition probabilities chosen such that $p_{eq}(S_i) \propto e^{-\beta \mathcal{H}(S_i)}$. One possible transition probability that generates this equilibrium probability is given by:

$$W_{i\to j} = \min\Big[1, \frac{\mathrm{p(S_j)}}{\mathrm{p(S_i)}}\Big]\,. \tag{4.36}$$

Here $p(S_j)$ and $p(S_i)$ are the actual probabilities for the system to be in state S_j or S_i given by $p(S_j) = \frac{1}{Z} e^{-\beta \mathcal{H}(S_j)}$. This transition probability satisfies detailed balance, as can be seen from inserting (4.36) into (4.35).

As mentioned before, one has to bear in mind that the partition function $Z = \sum_{allstates} e^{-\beta \mathcal{H}}$ is unknown. Anyhow, using the transition probability as defined in Equation (4.36) the partition function cancels out in Equation (4.37) and only the change in energy when passing from one configuration to the next matters

$$\frac{p(S_j)}{p(S_i)} = \frac{\frac{1}{Z}e^{-\beta\mathcal{H}(S_j)}}{\frac{1}{Z}e^{-\beta\mathcal{H}(S_i)}} = e^{-\beta(\mathcal{H}(S_j)-\mathcal{H}(S_i))}\,. \tag{4.37}$$

Applying Metropolis Algorithm in order to generate configurations within a canonical ensemble, the following scheme can be followed:

1. choose a random state as an initial configuration;
2. randomly pick one particle of all N particles;
3. propose a new configuration by performing a Monte-Carlo move (randomly changing the particles position and/or orientation);
4. calculate the energy difference between the old and the new configuration ΔU;
5. generate a random variable $r \in [0, 1]$ and accept the new configuration if $r < W_{old\to new}$.

Steps (2)-(5) are repeated several times. A set of N such repetitions is called a Monte-Carlo sweep. In order to generate configurations that show no unphysical correlations, one chooses to save a configuration only after a certain number of Monte-Carlo sweeps.

Chapter 5

Results

The simulations were carried out for four different system sizes. The different systems contained $N = 576, N = 900, N = 9216$ and $N = 82944$ particles. In the pre-study, the simulations were done on systems with 576 or 900 particles. In the following studies, I focused on the dimer case, where particles have patch amplitudes $\theta \in (0°, 60°)$, only for these systems the system size was increased to $N = 9216$ and $N = 82944$ particles.
Before I continue with presenting the results of the simulations and their analysis, I want to briefly explain the path I followed for the implementation of the model and for tackling the problems of saving computation time and going to larger system sizes.

5.1 Methodology for the Patchy Particle Model

Application of the Metropolis Algorithm

In my problem the N patchy colloids are restricted to closest spatial packing with periodic boundary conditions applied. The only degree of freedom left for a particle is its orientation. A configuration is therefore represented by a state in the N-dimensional subspace of phase-space given by a vector $\mathbf{X}^N = (\theta_1, \theta_2, ..., \theta_N)$. Applying the Metropolis Algorithm a rotation move is proposed to one randomly chosen particle where the rotation move is a rotation by a randomly generated angle. Then the transition probability from the old to the new configuration is calculated according to Equation (4.36). The new configuration is accepted or rejected according to this rule.
All results presented in the next chapter are based on simulations with $5 \cdot 10^5$ Monte-Carlo sweeps. One Monte-Carlo sweep consists of N proposed Monte-Carlo moves, where the particles for the rotation moves are picked randomly. After 500 sweeps, the full configuration (i.e. the orientations of all particles) was saved for the subsequent analysis. However the initial 10-20$\%$ of the configurations were discarded in order to sample only over the equilibrated system.
In the simulations either a cooling or a heating process was mimicked. Starting from

one particular configuration the temperature was subsequently lowered or raised by a small temperature increment. For each new temperature the last configuration of the previous temperature was taken to be the initial configuration for the simulation process. This is of course not the best option for many temperature steps because the process cannot be parallelized. A parallelized alternative, where every temperature is simulated independently from a random initial configuration, would however need longer to reach equilibrium.

Saving Computation Time

In an effort to save time during the simulation process the code was modified the following way. Each Monte-Carlo move is tested for acceptance by calculating the energy difference between the old and the new configuration. Since only one particle is rotated in each Monte-Carlo move, the calculation of the difference in energy can be restricted to the particle and its surrounding particles by introducing neighbour lists. In the case of my problem where the particles are fixed in their positions, this list must only be built once and never has to be updated as it would be the common procedure when using Verlet neighbour lists for simulation of liquids [1]. This strategy helps to save a considerable amount of simulation time since the potential function (2.1) does not have to be called for each pair of particles.

Passing to 82944 particles

In order to be able to perform simulations on considerably larger systems within a reasonable time, each temperature was simulated individually. The main obstacle was to decrease the time required for each simulation that gets lost during the equilibration process. For this purpose, the equilibrated configurations from the simulations with $N = 9216$ particles have been taken and replicated 9 times and put together into a system of nine times more particles, hence $N = 82944$. Thus I had an already equilibrated initial configuration for the further Monte-Carlo simulations at hand, leading to a smaller number of discarded configurations. For the previously described method, where for each Monte-Carlo move only the six surrounding particles are checked for changes in the energy, the correct neighbours have to be assigned to the particles on the border of the $N = 9216$ subsystems of the 9×9-grid.

5.2 Pre-Studies on the Bonding Patterns

5.2.1 Snapshots of Bonding Patterns

From first simulations on systems of $N = 900$ particles, snapshots of the bonding patterns at different temperatures were created. The system was simulated for 24

temperatures in the temperature interval $T \in [0.04, 0.5]$ in a cooling process with $5 \cdot 10^5$ Monte-Carlo sweeps at each temperature step.

Dimer Case

The number of bonds one particle can form depends on the patch amplitude θ according to Equation 2.3. When particles can form up to one bond ($n = 1$) figure 5.1 shows the bonding patterns at three different temperatures, $T = 0.28, 0.16$ and 0.04. The colors of the particles represent the number of bonds of the particle, where black particles are those which bonds are saturated.

Trimer Case

When n=2, the particles form up to two bonds each, here θ has to lie in the interval $(60°, 120°)$. The corresponding bonding patterns are trimers, dimers or lines. The snapshots in figure 5.2 are taken from simulations of two systems with different patch amplitudes: The first patch amplitude $\theta = 65°$ was chosen very close to the lower boundary while $\theta = 90°$ lies in the middle of interval.
For higher patch amplitudes the rotational entropy is higher than for lower patch amplitudes. Therefore, for $\theta = 90°$ the transition into the disordered phase takes place at a higher temperature when compared to the case with $\theta = 65°$. In figure 5.2 (f) the system has reached one possible groundstate where all bonds are saturated.
At the intermediate and higher temperatures also line structures (extending over three or more particles) occur. Here, it is the preferred phase compared to the trimer phase since the endpoints of the lines are able to contribute to a higher rotational entropy. However, at least in figure 5.2 (f) the line phase disappears completely in favour of the trimer phase, which has a far higher configurational entropy and is therefore much more likely to appear from the crystallization process.

Zigzag Case

For $n = 3$, figure 5.3 shows snapshots of two systems- one with patch amplitude $\theta = 125°$ and another with $\theta = 150°$. For the same entropic reason as discussed for the trimer case, the system with the smaller patch amplitude takes longer to crystallize. Again, one possible groundstate configuration is reached at $T = 0.04$ for the system with $\theta = 150°$ (Figure (5.3) (f)) : it consists of parallel left or right tilted zigzag lines. Due to the periodic boundary conditions, a groundstate with a kink in those zigzag lines would not be possible.

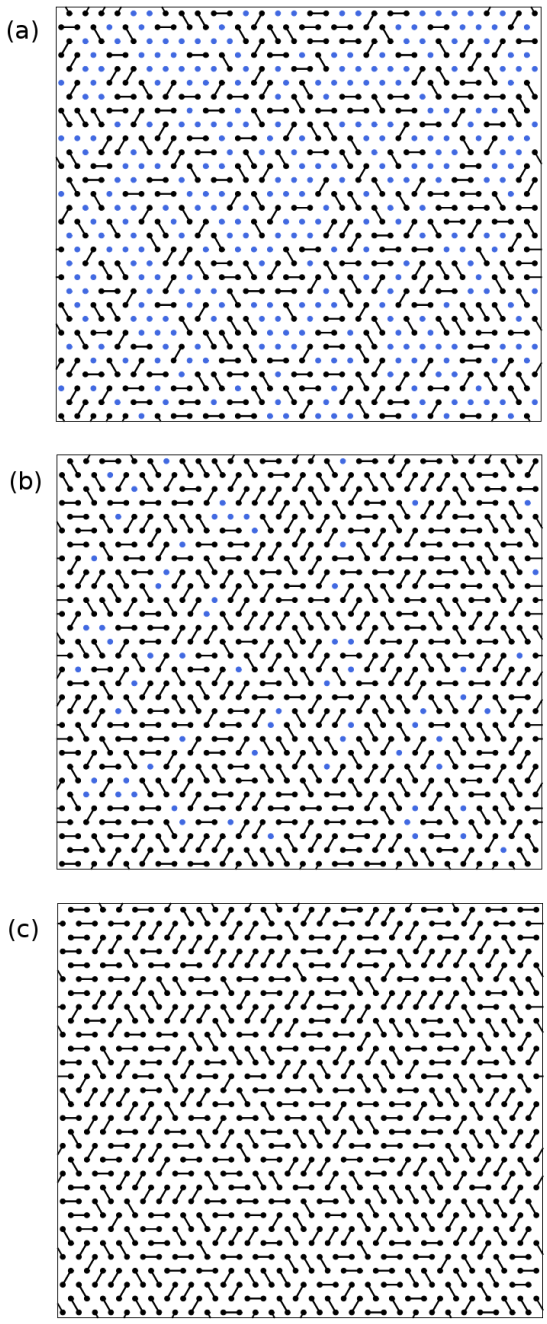

FIGURE 5.1: Simulation snapshots from a cooling process for N=900 particles with $\theta = 55°$ at temperatures (a) $T = 0.28$, (b) $T = 0.16$ and (c) $T = 0.04$.

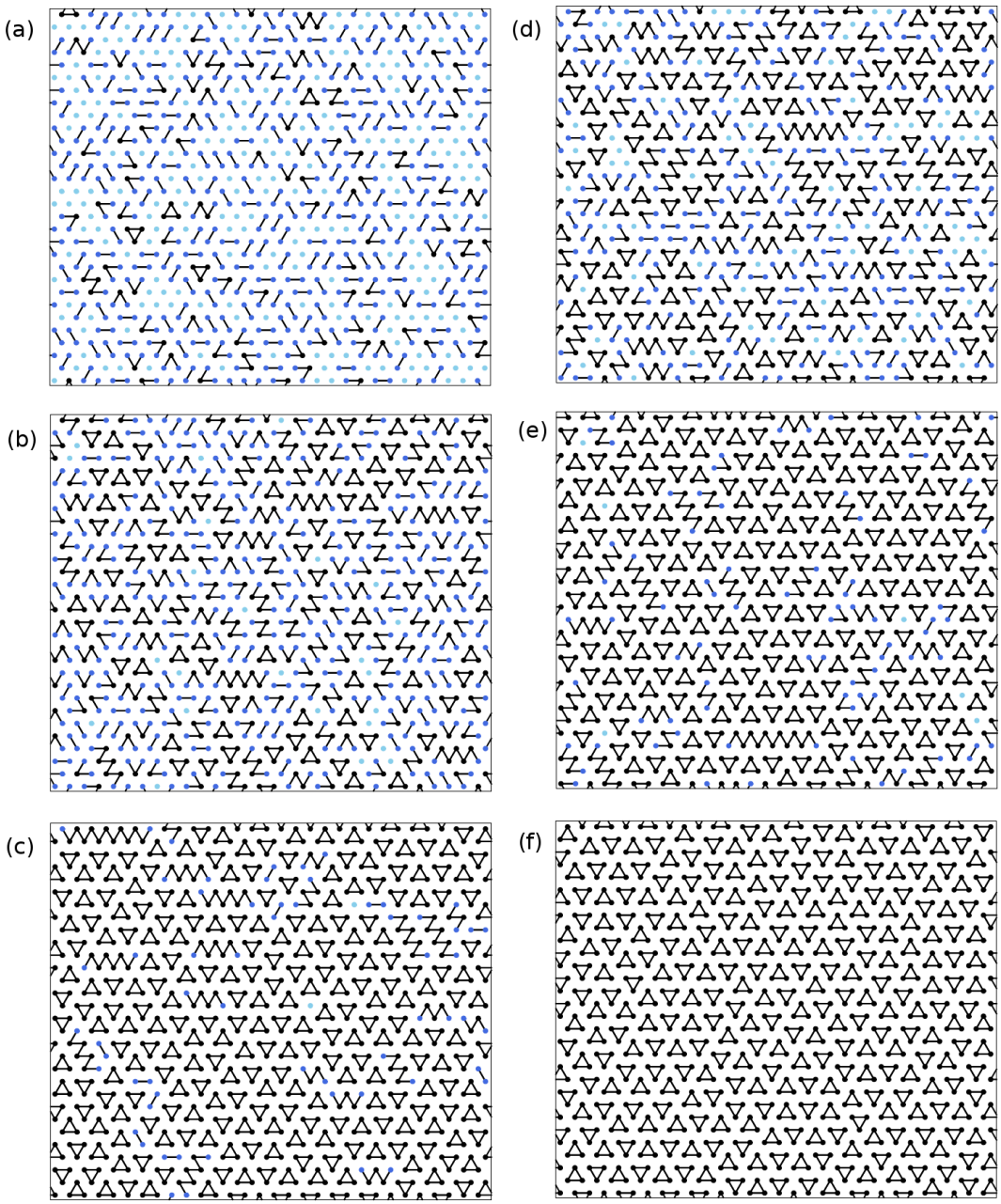

FIGURE 5.2: Simulation snapshots from a cooling process for N=900 particles with (a)-(c) $\theta = 65°$ and (d)-(f) $\theta = 90°$ at temperatures (a+d) $T = 0.28$, (b+e) $T = 0.16$ and (c+f) $T = 0.04$.

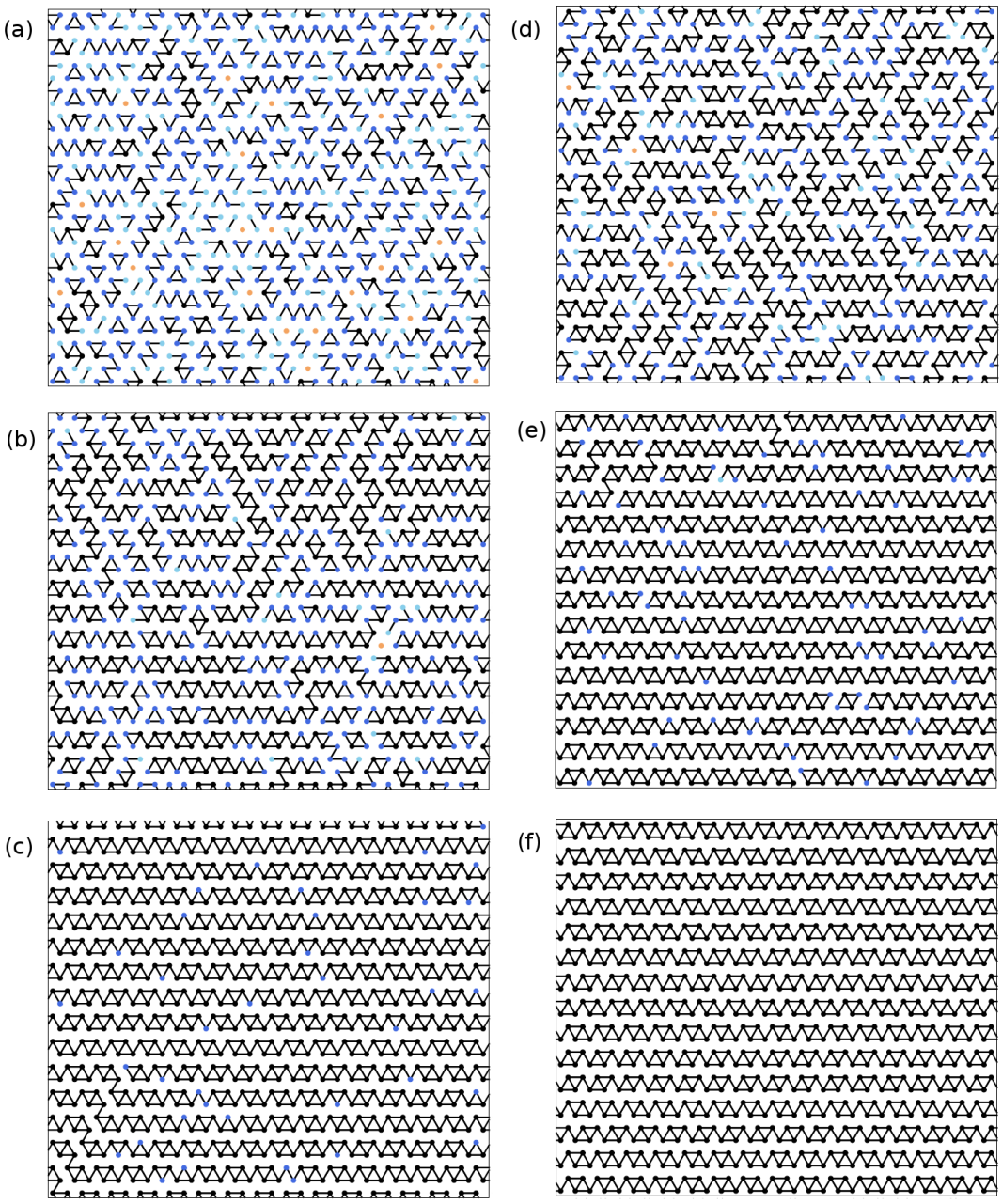

FIGURE 5.3: Simulation snapshots from a cooling process for N=900 particles with (a)-(c) $\theta = 125°$ and (d)-(f) $\theta = 150°$ at temperatures (a+d) $T = 0.28$, (b+e) $T = 0.16$ and (c+f) $T = 0.04$.

5.2.2 Density Analysis

The analysis in this section is based on the simulations with $N = 900$ particles presented in the previous section. With the density analysis, I want to calculate the densities of the emerging monomers, dimers and trimers. The density ρ_i for one of these structure indicated with index i are defined as:

$$\rho_i = \frac{n_i}{N}\,, \tag{5.1}$$

where n_i is the number of particles that are part of a structure i and N is the total number of particles in the system.

Dimer Case

In the analysis the densities of particles that are in a monomer or dimer configuration were determined by their energies. In a second step the full dimer density was divided into three densities of the different dimer types, which are horizontal, left and right tilted dimers.
Figure 5.4 shows the densities of monomers and dimers for different patch amplitudes as function of the temperature T. During the cooling process particles with larger patch amplitudes form dimers earlier than particles with smaller patch amplitudes because the entropic loss is not as high.

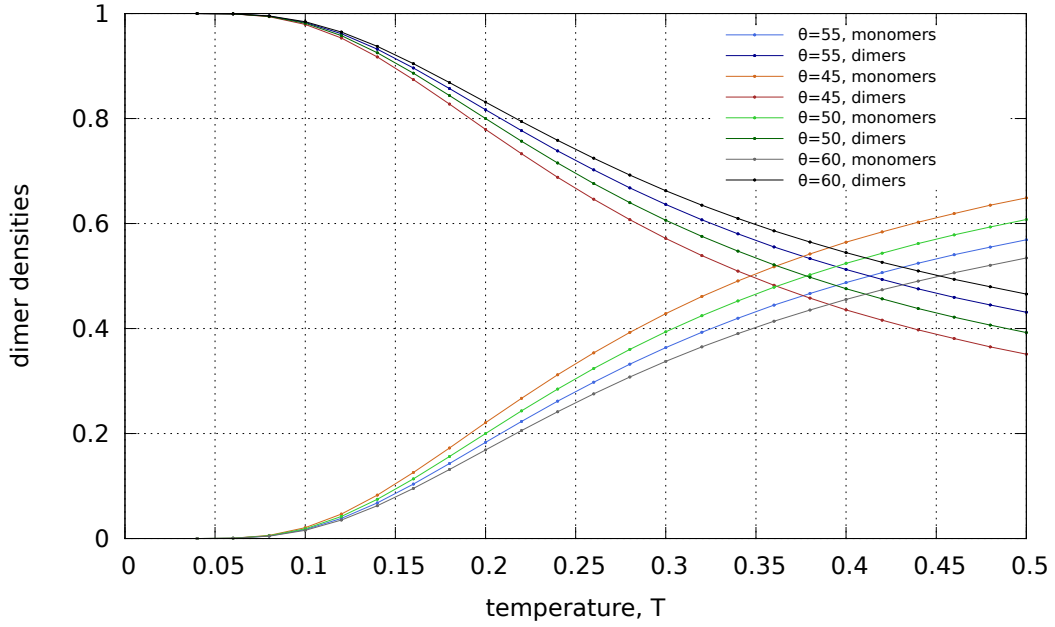

FIGURE 5.4: Monomer and dimer density analysis for systems with N=9216 particles at different patch amplitudes, obtained from a cooling process.

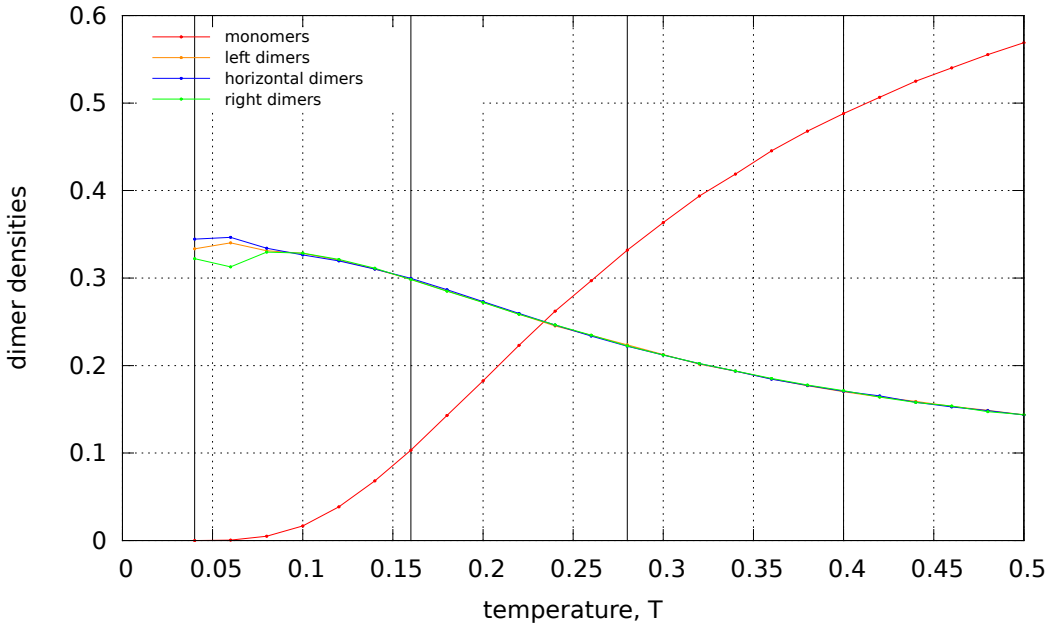

FIGURE 5.5: Densities of the different dimer types for system with N=900 particles and $\theta = 55°$, obtained from a cooling process.

In figure 5.5 also the densities for the horizontal, left and right tilted dimers in the case of a patch amlitude of $\theta = 55°$ are shown. The vertical lines mark the temperatures of the snapshots of the system showed in the figures 5.1. Of course these three types are symmetric and therefore the system would not favour a priori one of the directions. This is indeed observed at higher temperatures where due to a sufficiently large number of monomers the dimers seem to be completely independent. However, at low temperatures the curves split which happens due to the finite system size of the simulation box and a finite cooling time.

Trimer Case

Similar to the dimer case and inspired by [19], I distinguished in the analysis of the trimer densities six different types of trimers. In figure 5.6 these six trimer types are indicated in a hexagonal cell of the trigonal lattice.

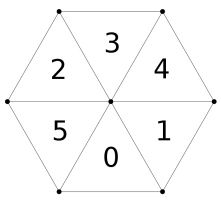

FIGURE 5.6: Six sublattices of the trigonal lattice

In [19] an analytical derivation of the entropy for the trimer problem is presented. The trimer problem is stated as a tiling of trimers that covers all lattice sites of an underlying trigonal without overlaps. In [19] the trigonal lattice was split into six sublattices, where each sublattice represents one trimer type. A fully occupied sublattice represents a special solution to the tiling problem because it possesses

a discrete translational symmetry into the two directions of the two-dimensional lattice. By a Bethe ansatz the authors were able to derive the entropy and the densities of the sublattices $\rho_0, ..., \rho_5$. The six trimer types can also be grouped into down-oriented trimers and up-oriented trimers with densities $\rho_\nabla = \rho_1 + \rho_3 + \rho_5$ and $\rho_\Delta = \rho_0 + \rho_2 + \rho_4$.

The most important findings that were delivered via this analytical approach were that the entropy of the system is maximal if the up- and down-trimers are balanced, $\rho_\nabla = \rho_\Delta$. And secondly that a spontaneous symmetry breaking takes place if one of these densities gets small compared to the other, e.g. $\rho_\nabla < \rho_\Delta$. In this case, the symmetry between the three trimer types that make up ρ_Δ is spontaneously broken as one type increases, e.g. $\rho_0 > \rho_1 = \rho_3 = \rho_5 > \rho_2 = \rho_4$. However this spontaneous symmetry breaking mainly plays a role if the up- and down-trimer densities could be regulated. In my problem this is not the case. The density calculation in

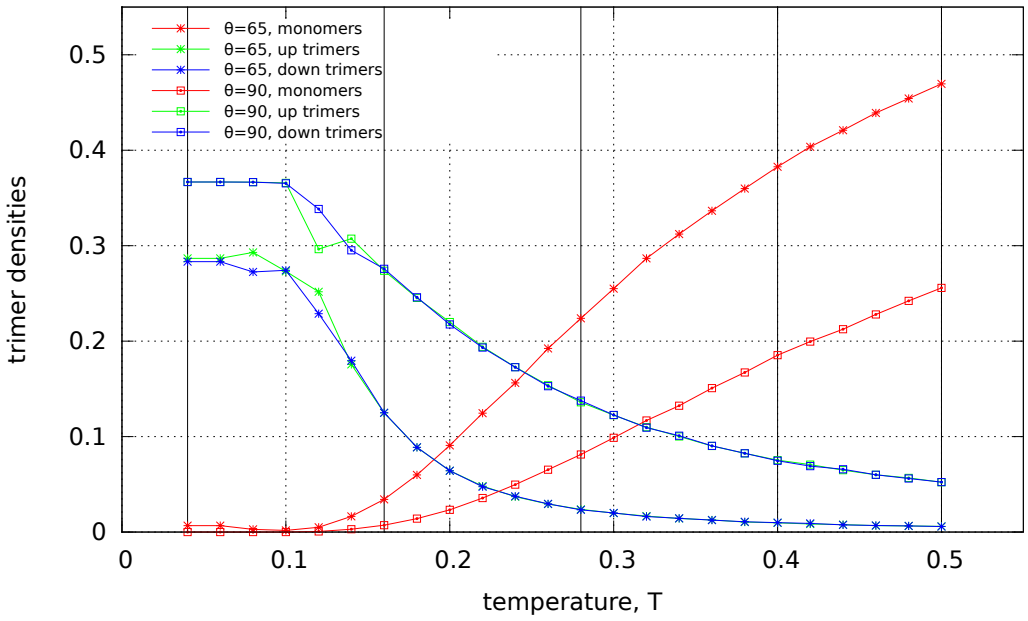

FIGURE 5.7: Trimer density analysis for systems with N=900 particles at different patch amplitudes, obtained from a cooling process.

this work was carried out for the two previously presented systems with $N = 900$ particles and patch amplitudes $\theta = 65°$ and $\theta = 90°$. In figure 5.7 the up- and down-trimer densities are considered separately for these two cases.

As expected, the densities ρ_∇ and ρ_Δ become equal when $\theta = 90°$. Only here, all monomers disappear at low temperatures and a ground state is reached. As derived by [19] equal densities for up- and down-trimers has the highest entropy and is therefore most likely to occur. For $\theta = 65°$ the ground state is not yet reached since the monomer density is still non-zero. The next figures, (5.8) and (5.9), show the densities of all six trimer types for the two systems. In the density calculation,

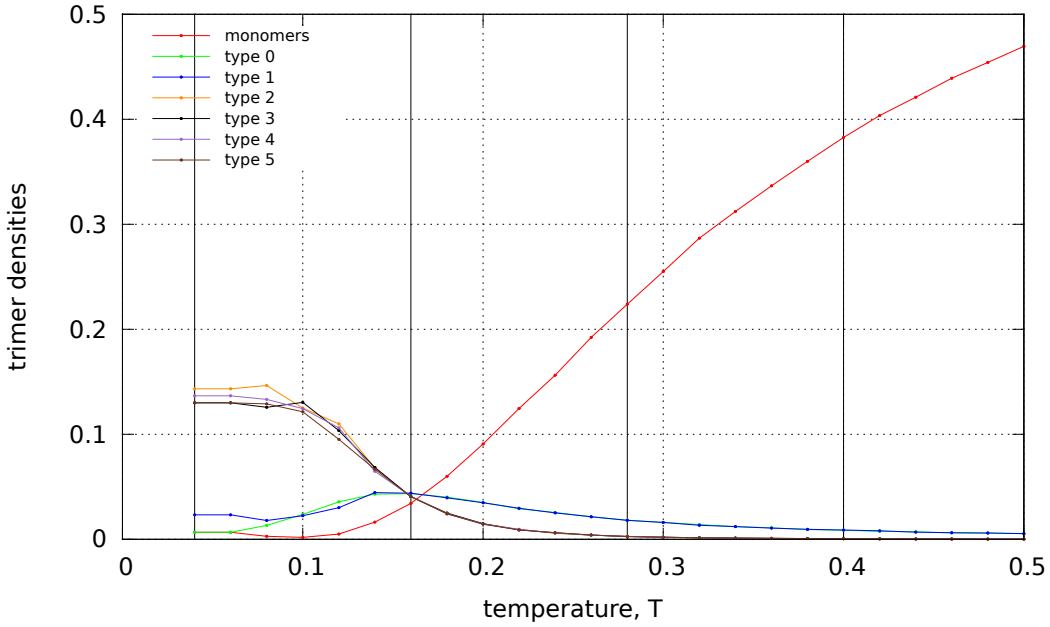

FIGURE 5.8: Trimer density analysis for system with N=900 particles and $\theta = 65°$, obtained from a cooling process.

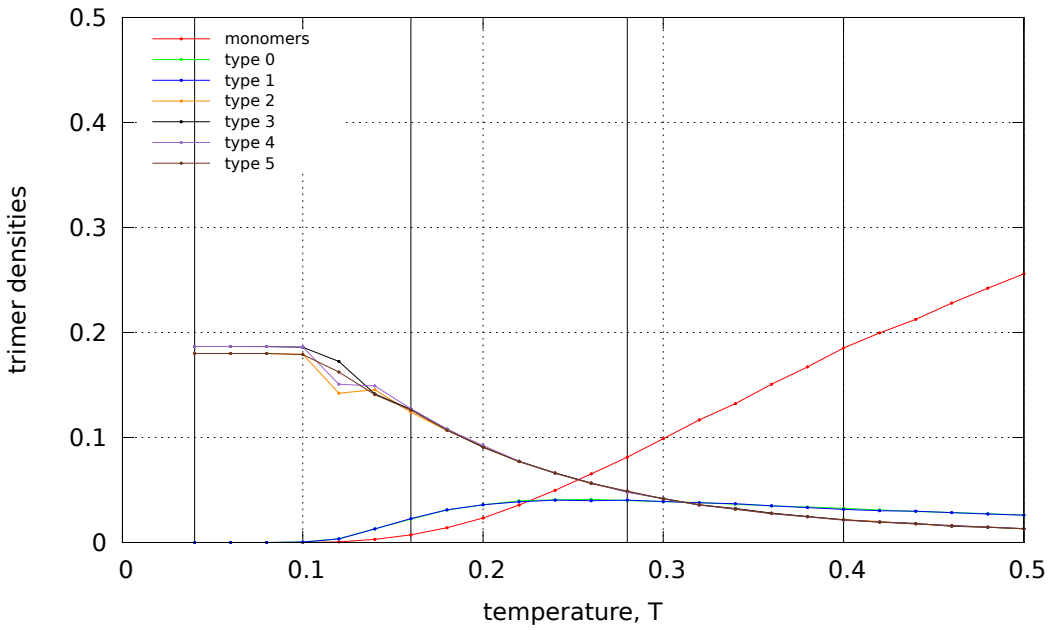

FIGURE 5.9: Trimer density analysis for system with N=900 particles and $\theta = 90°$, obtained from a cooling process.

the six trimer types were distinguished and plotted individually. As it can be seen from figure (5.7) the up- and down-trimers have the same densities for higher temperatures. This is obvious since they represent symmetric states and are completely independent of each other as long as the monomer density is high enough. As soon as the monomers disappear the trimers get trapped in one configuration.
From the analytical derivation of the free energy and of the entropy of a system of trimers with the constraint that they have to cover the lattice completely [19], it is known that balanced densities $\rho_{\triangledown}$ and $\rho_{\triangle}$ of up- and down-trimers leads to the highest entropy.

The fact, that at low temperatures the density curves for up- and down-trimers split has to do with trapped configuration. Simulations with slower cooling processes and higher system sizes would most likely end up in the configuration of highest entropy where all the sub-densities are balanced.

5.2.3 Cluster Size Analysis

In the density analysis for the trimer case only trimers, dimers and monomers were distinguished. By the use of a cluster size analysis, also lines formed by three or more particles as they can be seen in figure 5.2 could be tracked. A standard cluster size analysis was implemented. Solely clusters of size three were distinguished into two different cluster types, trimers and open triangles, which are lines of three particles.
Figures 5.10 and 5.11 show the densities of monomers, dimers, trimers and line structures as defined in equation 5.1 for the two considered angles $\theta = 65^\circ$ and $\theta = 90^\circ$.
From figure 5.11 it can be seen that the system reaches a ground state in the pure trimer phase. When looking at the densities of the line structures it becomes obvious that for all temperatures the shorter lines are more likely to emerge than the longer ones. But as the lines get larger, the maximal probability for each line type gets to lower temperatures. The reason for this behaviour can be found when considering the competing of the energy and entropy at the ends of the line.

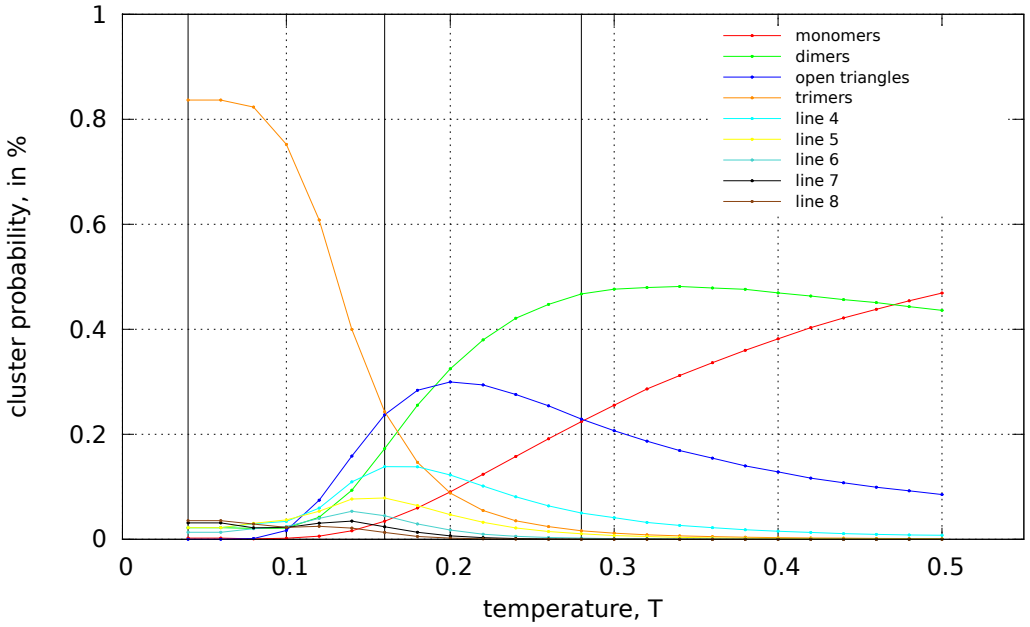

FIGURE 5.10: Cluster size analysis on system with N=900 particles and $\theta = 65°$, obtained from cooling process.

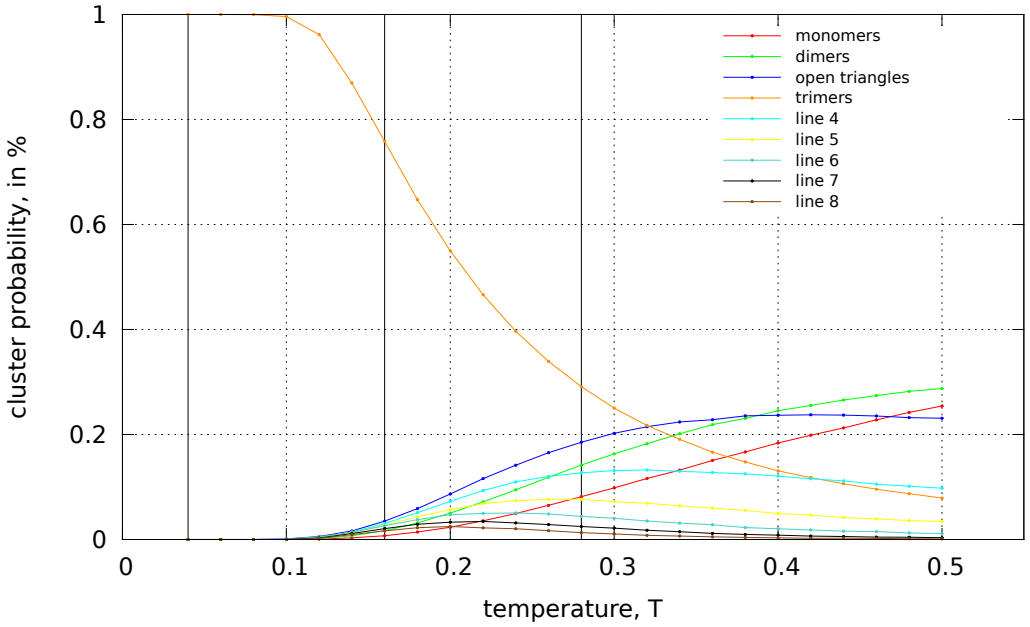

FIGURE 5.11: Cluster size analysis on system with N=900 particles and $\theta = 90°$, obtained from cooling process.

5.3 Detailed Studies on the Dimer Case

For the further analysis I focused on the system with $\theta = 55°$. From the results of the density analysis on this system, I located the transition temperature to lie in the interval $[0.04 - 0.08]$. As it can be seen from figure 5.4 the first monomers emerge in this interval and the transition from the ordered phase into the disordered sets in. The increment in temperature, ΔT was assumed to be 0.001.

5.3.1 Energy per Particle as the Order Parameter

As suggested in section 2.3 the *global* order parameter for the dimer phase is simply the energy per particle ϵ. However this choice will not provide new information since the ϵ- curve will reproduce the monomer curve shown in figure 5.4 shifted in the $y-$direction by -1. Nevertheless, I performed the analysis in the smaller temperature window and went to higher system sizes. In figure 5.12 the averaged energy per particle $\langle\epsilon\rangle$ is presented with the respective statistical errors for the three different system sizes investigated.

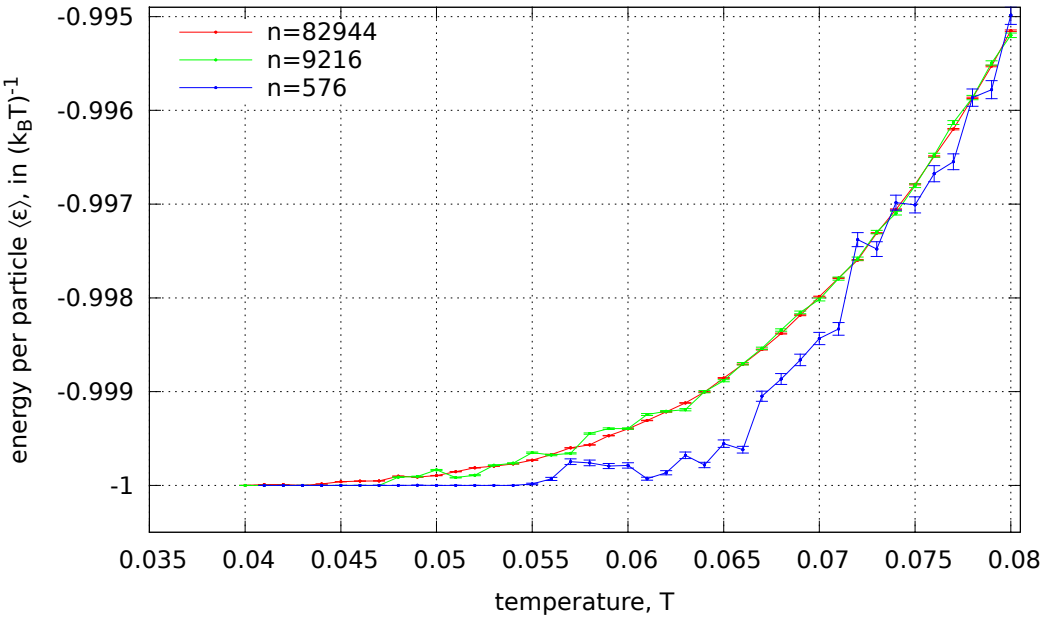

FIGURE 5.12: Global order parameter $\langle\epsilon\rangle$ with errorbars, comparison for different system sizes.

5.3.2 Energy Autocorrelation Function

In the next step the correlation function of the *local* order parameter has been investigated. As the local order parameter the energy $\epsilon(\vec{r}_i)$ of a particle at position $\vec{r}_i$ can be defined. Then the correlation of the local order parameter of two particles separated

by a distance r is given by:

$$g(r = |\vec{r}_{ij}|) = \langle \epsilon(\vec{r}_i)\epsilon(\vec{r}_j)\rangle = \frac{1}{2N} \sum_{\text{allconf}} \sum_{\substack{i,j \\ r=|\vec{r}_{ij}|}} \epsilon(\vec{r}_i)\epsilon(\vec{r}_j)\,, \tag{5.2}$$

with the normalization factor,

$$N = \sum_{\text{allconf}} \sum_{\substack{i,j \\ r=|\vec{r}_{ij}|}} 1\,. \tag{5.3}$$

The average denoted by $\langle\cdot\rangle$ is taken over all configurations and all particles at positions $\vec{r}_i$ and $\vec{r}_j$ with the restriction that the particles at these positions have distance r. The normalization factor is the number configurations times the number of all pairs of particles separated by a distance r that can be found in one configuration.
In figure 5.13 this correlation function of the order parameter calculated from the largest system with $N = 82944$ particles is plotted for distances up to 20 particle diameters at different temperatures. The temperatures range within the interval $[0.04 - 0.08]$. The correlation function as a function of the distance is constant, and also stays constant for larger distances, at the temperatures shown from the first neighbour particles on. But for higher temperatures the constant value decreases since bonds start to break. The order of the correlation is thus quasi long-range.
In figure 5.14 the same correlation function is plotted for higher temperatures ranging within the interval $[0.08-0.4]$. For the first three shells around the central particle some oscillations appear which indicate a very short range effective interaction between the dimers.

5.3.3 Heat Capacity

The heat capacity at constant volume C_V is a response function which is able to provide information about the possible occurrence of a phase transition.
There are two common methods for determining the heat capacity from simulations in the NVT-ensemble. The first method starts from the definition of the heat capacity at constant volume,

$$C_V = \Big(\frac{\partial Q}{\partial T}\Big)_V = \frac{\partial U}{\partial T} \tag{5.4}$$

The energy U is determined from the simulations as an average $\langle U\rangle_{T_i}$ for each temperature T_i in the simulation process. When fitting a function through the data and then taking the derivative of this fit-function with respect to T the heat capacity at constant volume can then be calculated.

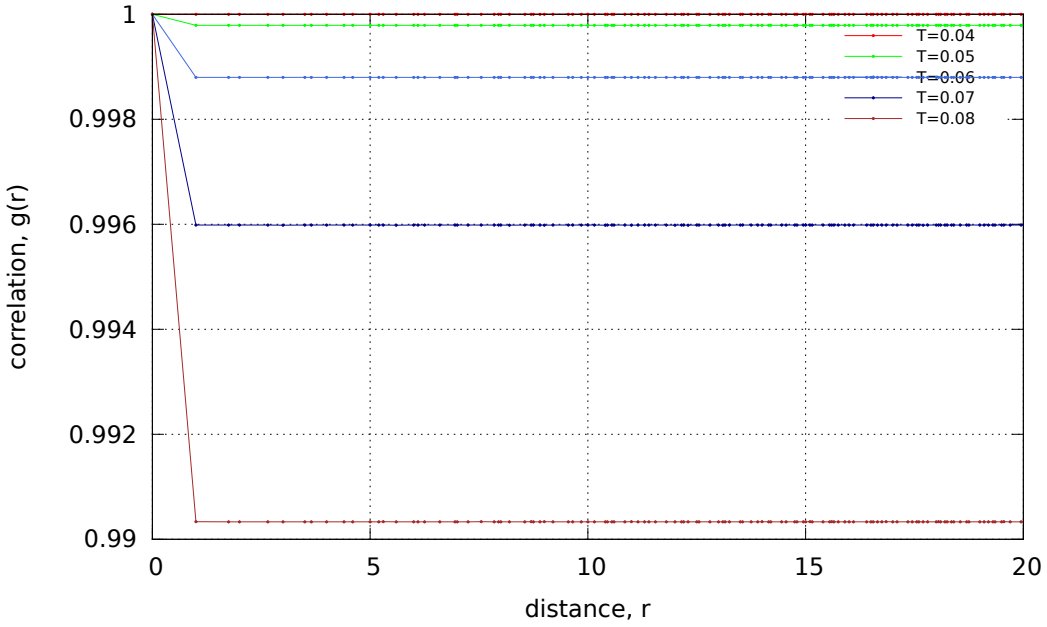

FIGURE 5.13: Correlation function of the local order parameter $g(r)$ at different temperatures for system of $N = 82944$ particles with $\theta = 55°$.

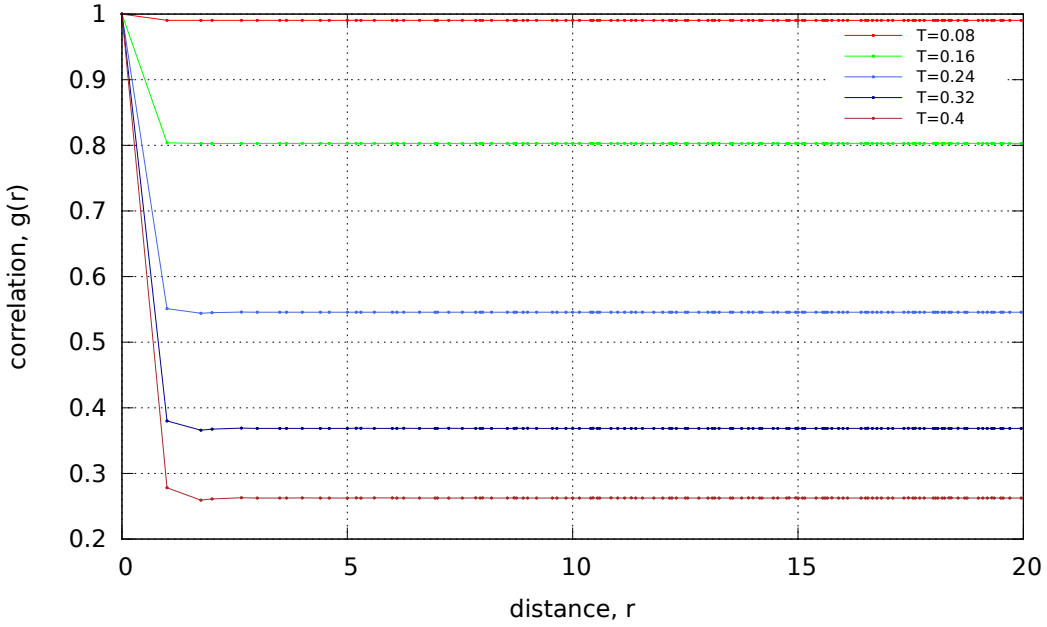

FIGURE 5.14: Correlation function of the local order parameter $g(r)$ for higher temperatures calculated from system of $N = 9216$ particles with $\theta = 55°$.

An alternative method is to use formula (4.23). Via this approach, the heat capacity at constant volume can be calculated from the energy fluctuations $\langle \mathcal{H} \rangle^2 - \langle \mathcal{H}^2 \rangle$ during the simulation process. This method was used in the following analysis. Although being very attractive for the fact that the heat capacity can be directly measured from the simulations, this method has the disadvantage that very good statistics are needed to obtain smooth data for C_V. From figure 5.15 it can be seen that even for the largest system of $N = 82944$ particles the curve is still not able to give reasonable results.

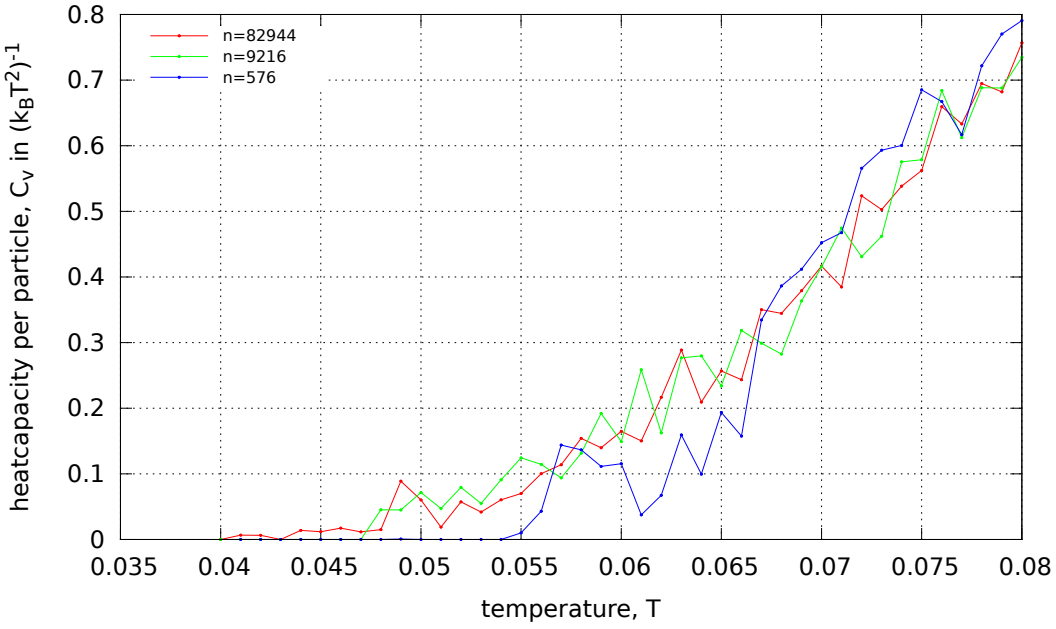

FIGURE 5.15: Heatcapacity at constant volume calculated from energy fluctuations, comparison for different system sizes.

Chapter 6

Conclusion & Outlook

At the beginning of this work stood the melting transition of colloid particles in two dimensions. For this system a microscopic theory for melting has been developed by Kosterlitz, Thouless, Haperlin, Nelson and Young in the 1970s. The predictions of this theory, particularly the occurrence of a hexatic phase which occurs between the solid and the liquid phase have been proven many times in experiments and simulations.

For this work, I extended the model of the colloid particles by assigning a patch with an attractive interaction to the otherwise repulsive surface of the particles. Through this patch the particles have an additional, orientational degree of freedom.
The original idea of this thesis was to investigate this system by first of all clarifying whether it still undergoes a KTHNY melting transition and secondly determining how this melting transition is related to the order-disorder transition of the orientational order. As a first step to pursue this issue the orientational order transition was disentangled from the spatially induced melting transition. In order to realize this, the particles were restricted to closest spatial packing, thus allowing the particles only to rotate.

In the course of my studies I focused primarily on the cases where particles can form one or two bonds. The aim was to gain more knowledge on how to treat this problem also for those cases, where the particles can form more bonds. This part of the work comprised density and cluster size analyses of the emerging bonding structures in the dimer and trimer case.
For the dimer case a local order parameter was defined which was found to be modulus of the energy of each particle. Using this order parameter the correlation of the local order parameter was calculated in order to investigate the range of order in the different phases. To be able to study long range order also simulations on larger systems were performed. Anyhow, so far I was not able to draw any clear conclusions from the obtained results.
The heat capacity was determined from the fluctuations in the energy during the

simulation for the dimer case. For now, the heat capacity curve has large fluctuations because even for the largest system the statistics are apparently of insufficient quality. From these results no conclusions can be drawn yet. For this analysis even larger system sizes or longer simulation runs are needed to get better statistics.

The next steps will be to find one single or a set of suitable order parameters for the trimer case in order to distinguish the trimers, line structures and monomers from each other. On the basis of these order parameters, the range of order in the different phases can be studied using the correlation functions of the respective order parameters.
If the phase transition of the orientational order for the case of closest spatial packing is better understood, it will be interesting to proceed further and also let the system undergo a melting transition. The melting transition of the patchy colloids can then be compared to the KTHNY phase transition of usual colloid particles. Finally, the original research question can be tackled by studying the phase transitions of the differently orientationally ordered phases in combination with the melting transition. For this purpose the order parameters that were found for the case of highest packing fractions might be useful to define orientationally ordered phases in this somewhat different problem.

Bibliography

[1] M. P. Allen and Dominic J. Tildesley. *Computer simulation of liquids*. Clarendon Press, 1987. ISBN: 0198556454.

[2] Paul M. Chaikin and T. C. Lubensky. *Principles of condensed matter physics*. Cambridge University Press, 1995, p. 699. ISBN: 0521794501.

[3] S. T. Chui. "Grain-boundary theory of melting in two dimensions". In: *Physical Review B* 28.1 (1983), pp. 178–194. DOI: 10.1103/PhysRevB.28.178. URL: http://link.aps.org/doi/10.1103/PhysRevB.28.178.

[4] Michael Engel et al. "Hard-disk equation of state: First-order liquid-hexatic transition in two dimensions with three simulation methods". In: *Physical Review E* 87.4 (2013), p. 042134. ISSN: 1539-3755. DOI: 10.1103/PhysRevE.87.042134. URL: http://link.aps.org/doi/10.1103/PhysRevE.87.042134.

[5] Enrico Fermi. *Thermodynamics*. 1957. URL: http://linkinghub.elsevier.com/retrieve/pii/B978012654680450007$\backslash$npapers3://publication/doi/10.1016/b978-0-12-654680-4.50007-0.

[6] Matthew A. Glaser and Noel A. Clark. "Melting and Liquid Structure in two Dimensions". In: John Wiley & Sons, Inc., pp. 543–709. ISBN: 9780470141410. DOI: 10.1002/9780470141410.ch7. URL: http://doi.wiley.com/10.1002/9780470141410.ch7.

[7] Hans Hennig von Grünberg, Peter Keim, and Georg Maret. "Phase transitions in two-dimensional colloidal systems". In: *Colloidal order : entropic and surface forces*. Ed. by Gerhard Gompper. Soft matter 3. Weinheim: WILEY-VCH, 2007, pp. 40–83. ISBN: 978-3-527-31370-9.

[8] Y. Iwashita and Y. Kimura. "Orientational order of one-patch colloidal particles in two dimensions". In: *Soft Matt.* 10.37 (2014), DOI:10.1039/C4SM00932K. ISSN: 1744-6848. DOI: 10.1039/C4SM00932K. URL: http://dx.doi.org/10.1039/C4SM00932K.

[9] Norbert Kern and Daan Frenkel. "Fluid–fluid coexistence in colloidal systems with short-ranged strongly directional attraction". In: *The Journal of Chemical Physics* 118.21 (2003), pp. 9882–9889. ISSN: 0021-9606. DOI: 10.1063/1.

1569473. URL: http://aip.scitation.org/doi/10.1063/1.1569473.

[10] H. Kleinert. "Disclinations and first order transitions in 2D melting". In: *Physics Letters A* 95.7 (1983), pp. 381–384. ISSN: 03759601. DOI: 10.1016/0375-9601(83)90413-9.

[11] J Michael Kosterlitz and D J Thouless. "Ordering, metastability and phase transitions in two-dimensional systems". In: *Journal of Physics C: Solid State Physics* 6 (1973), pp. 1181–1203. ISSN: 0022-3719. DOI: 10.1088/0022-3719/6/7/010. URL: http://iopscience.iop.org/0022-3719/6/7/010.

[12] David P. Landau and K. (Kurt) Binder. *A guide to Monte Carlo simulations in statistical physics*. 3rd ed. Cambridge University Press, 2009, p. 471. ISBN: 0521768489.

[13] Vasilios I Manousiouthakis and Michael W Deem. "Strict Detailed Balance is Unnecessary in Monte Carlo Simulation". In: *J. Chem. Phys* (1998). arXiv: 9809240v2 [arXiv:cond-mat].

[14] Xiaoming Mao, Qian Chen, and Steve Granick. "Entropy favours open colloidal lattices". In: *Nature Materials* 12 (2013), p. 217. DOI: 10.1038/NMAT3496.

[15] Nicholas Metropolis et al. "Equation of State Calculations by Fast Computing Machines". In: *The Journal of Chemical Physics* 21.6 (1953), pp. 1087–1092. DOI: 10.1063/1.1699114. URL: http://aip.scitation.org/doi/10.1063/1.1699114.

[16] L. E. Reichl. *A modern course in statistical physics*. Fourth rev. 2016, p. 467. ISBN: 3527413499.

[17] Franz Schwabl. *Statistical Mechanics*. Vol. 126. Springer-Verlag Berlin Heidelberg GmbH, 1997. ISBN: 9783642629020. DOI: 10.1007/978-3-662-04482-7.

[18] Homin Shin and Kenneth S Schweizer. "Soft Matter Theory of two-dimensional self-assembly of Janus colloids: crystallization and orientational ordering". In: *Soft Matter* 10.2 (2014), pp. 229–400.

[19] Alain Verberkmoes and Bernard Nienhuis. "Triangular Trimers on the Triangular Lattice: an Exact Solution". In: *Physical Review Letters* 83.20 (1999), p. 4. ISSN: 0031-9007. DOI: 10.1103/PhysRevLett.83.3986. URL: http://arxiv.org/abs/cond-mat/9904343.

[20] A P Young. "Melting and the vector Coulomb gas in two dimensions". In: *Physical Review B* 19.4 (1979), pp. 1855–1866. ISSN: 01631829. DOI: 10.1103/PhysRevB.19.1855. arXiv: arXiv:1011.1669v3.